

AD-A230 186

Annual Letter Report

**Growth, Characterization and Device Development in
Monocrystalline Diamond Films**

Supported by the Innovative Science and Technology Office
Strategic Defense Initiative Organization
Office of Naval Research
under Contract #N00014-90-J-1604
for the period January 1, 1990–December 31, 1990

Robert F. Davis, Jeffrey T. Glass, Klaus J. Bachmann, and R. J. Trew*
North Carolina State University
c/o Materials Science and Engineering Department and
*Electrical and Computer Engineering
Raleigh, NC 27695-7907

December 31, 1990

12

DEC 20 1990
CO 9

AD-A230 186

REPORT DOCUMENTATION PAGE

Form Approved
OMB No 0704-0188

Public reporting burden for this collection of information is estimated to average 1 hour per response, including the time for reviewing instructions, searching existing data sources, gathering and maintaining the data needed, and completing and reviewing the collection of information. Send comments regarding this burden estimate or any other aspect of this collection of information, including suggestions for reducing this burden to: Washington Headquarters Services, Directorate for Information Operations and Reports, 1215 Jefferson Davis Highway, Suite 1204, Arlington, VA 22202-4302 and to the Office of Management and Budget, Paperwork Reduction Project (0704-0188), Washington, DC 20503

1. AGENCY USE ONLY (Leave blank)	2. REPORT DATE December, 1990	3. REPORT TYPE AND DATES COVERED Annual 1/1/90-12/31/90
----------------------------------	----------------------------------	--

4. TITLE AND SUBTITLE Growth, Characterization and Device Development in Monocrystalline Diamond Films	5. FUNDING NUMBERS s400003srr08 1114SS N00179 N66005 4B855
---	---

6. AUTHOR(S) Robert F. Davis	
-------------------------------------	--

7. PERFORMING ORGANIZATION NAME(S) AND ADDRESS(ES) North Carolina State University Hillaborough Street Raleigh, NC 27695	8. PERFORMING ORGANIZATION REPORT NUMBER N00014-90-J-1604
---	--

9. SPONSORING/MONITORING AGENCY NAME(S) AND ADDRESS(ES) Department of the Navy Office of the Chief of Naval Research 800 North Quincy Street, Code 1513:CMB Arlington, VA 22217-5000	10. SPONSORING/MONITORING AGENCY REPORT NUMBER
--	--

11. SUPPLEMENTARY NOTES

12a. DISTRIBUTION/AVAILABILITY STATEMENT Approved for Public Release; Distribution Unlimited	12b. DISTRIBUTION CODE
---	------------------------

13. ABSTRACT (Maximum 200 words)

In this reporting period, diamond films have been deposited on various polycrystalline metal and (001) Si substrates by biased hot filament chemical vapor deposition, the films characterized by TEM, x-ray diffraction and Raman and Auger spectroscopies and MESFET devices modeled from the properties of diamond. In addition Cu single crystals were implanted at 900°C with C ions and other studies initiated in an attempt to achieve heteroepitaxial growth of diamond. Films grown on Si, Ni and W exhibited the highest quality diamond films from the viewpoint of Raman characterization. The model of the MESFET device with gate length = 1 micron and width = 1 mm showed that significant degradation in RF performance is not expected at 10 GHz. The implanted C species diffused to the surface of the Cu (100) crystals as predicted, but graphite was the resultant phase. Other implantation and high pressure studies are described as attempts to obtain monocrystalline diamond films.

14. SUBJECT TERMS 25 diamond thin films, chemical vapor deposition, Raman spectroscopy, electronic devices, MESFETs, ion implantation high pressure studies, epitaxial regrowth, amorphous C films	15. NUMBER OF PAGES 59
	16. PRICE CODE

17. SECURITY CLASSIFICATION OF REPORT UNCLAS	18. SECURITY CLASSIFICATION OF THIS PAGE UNCLAS	19. SECURITY CLASSIFICATION OF ABSTRACT UNCLAS	20. LIMITATION OF ABSTRACT SAR
---	--	---	-----------------------------------

Table of Contents

- I. Bias Controlled Hot Filament Chemical Vapor Deposition of Diamond Thin Film on Various Substrates
- II. Electron Microscopic Characterization of Diamond Films Grown on Si by Bias-Controlled Chemical Vapor Deposition
- III. Novel Approaches to the Attainment of the Heteroepitaxy of Diamond Films
- IV. Electronic Devices Fabricated From Diamond
- V. Appendix—Distribution List



Accession For		↓
NTIS	CRA&I	☐
DTIC	TAB	☐
Unannounced		☐
Distribution		
By		
Distribution		
Availability Codes		
Dist	Availability Code	Special
A-1		

I. BIAS CONTROLLED HOT FILAMENT CHEMICAL VAPOR DEPOSITION OF DIAMOND THIN FILM ON VARIOUS SUBSTRATES

Y. H. LEE, G.-H. MA, K. J. BACHMANN and J. T. GLASS

North Carolina State University, Materials Science and Engineering Department, Raleigh, NC 27695-7907

ABSTRACT

The growth of diamond films on Si(001), polycrystalline Ni, Mo, Ta, and W substrates by biased controlled chemical vapor deposition is discussed. Biasing effects were examined using the Si(001) substrates. The film quality as judged by Raman spectroscopy and scanning electron microscopy depended strongly on the biasing conditions. Under low current reverse bias conditions, highly faceted cubooctahedral polycrystalline diamond growth exhibiting a single sharp Raman line at 1332 cm^{-1} was obtained. Transmission electron microscopy indicated that these films contained relatively low defect densities and no significant interfacial layers. Biasing into high current conditions which created a plasma resulted in multiply twinned, microcrystalline growth incorporating sp^2 bonded carbon into the diamond film. Such films were found to contain very high defect densities and a relatively thick interfacial layer. An investigation of the effects of substrate material was also conducted. Films grown on Si, Ni and W exhibited the best quality. The relationship between this quality and substrate properties such as surface energy and lattice parameter is discussed.

INTRODUCTION

Diamond films and particles have been grown by various deposition methods [1-7] for both electronic and mechanical applications. Charged species, especially electrons, may play a significant role during the hot filament CVD of diamond. For example, electrons may damage the surface of diamond [8] or they may accelerate the decomposition of H_2 and CH_4 [3], each yielding opposite effects in terms of film quality. Thus, the effects of biasing during diamond CVD are of utmost interest. Also, economic considerations will require the development of reasonably large non-diamond substrates for the growth of diamond films. Therefore, the influence of substrate materials on diamond growth must be understood. In the present research the biasing conditions and substrate materials which result in well-faceted growth morphology and sharp Raman spectra characteristic of pure diamond are described.

EXPERIMENTAL CONDITIONS

Bias Controlled CVD

The experimental arrangement of the Bias Controlled Chemical Vapor Deposition (BCCVD) system utilized in the present study is similar to conventional hot filament CVD systems [1]. However, means have been added for independent biasing of the substrate and the filament with regard to the grounded walls of the growth chamber which is discussed in more detail elsewhere [6,7]. Si(001) substrates

were mechanically polished with diamond paste to a final grit size of 0.25 μm . The methane to hydrogen ratio was fixed at 3%, total flow at 100 sccm, and pressure at 3.3 kPa. The filament and substrate temperatures were 1930 $^{\circ}\text{C}$ and 850 $^{\circ}\text{C}$, respectively and the filament to substrate distance was 8 mm. In experiments of biasing effects, only the bias was varied. Initial experiments involved the variation of the filament bias voltage and substrate bias voltage independently relative to the grounded chamber. However, it was found that the current depended primarily on the potential difference (ΔV) between the filament and substrate due to the highly resistive path to the chamber walls which were on the order of 3 cm away. Furthermore, it was found that relative to this ΔV , the system behaves like a diode due to the high temperature of the filament which easily ejects electrons versus the low temperature of the substrate which does not allow the electrons to escape easily. Thus, "forward" bias is defined as the condition in which the substrate is held at a positive potential relative to the filament (i.e., electrons flowing into the substrate) and "reverse" bias is defined as the opposite condition to forward bias [7]. At high reverse bias ($\geq 170\text{V}$) and moderate forward bias ($\geq 70\text{V}$) the current flow increased suddenly indicating that a plasma was generated. Silicon(001) substrates were utilized and the deposited films were characterized by SEM, Raman spectroscopy and TEM.

Substrate Variations

During this substrate variation study, diamond was deposited on several substrates under reverse bias ($\sim 120\text{V}$) which was found to be optimum in the biasing study. In addition to Si(001), polycrystalline metal substrates were evaluated using the same surface finish. These substrates were chosen for the following reasons: (i) Si is a material with the diamond structure and has an excellent thermal expansion coefficient match with diamond, (ii) Ni is closely lattice-matched to diamond, (iii) refractory metals such as Mo, Ta and W are strong carbide formers with relatively high surface energies (i.e., relatively close to diamond) and thus are expected to result in relatively small interfacial energies between the diamond nuclei and the substrate.

RESULTS AND DISCUSSION

Bias Controlled CVD

The film quality as judged by Raman spectroscopy depends strongly on the biasing conditions, as shown in Figure 1. It can be seen that in the low current reverse biasing condition (Figure 1c), only the 1332 cm^{-1} diamond line is observed. The broad band normally located at $\sim 1500 \text{ cm}^{-1}$ typically associated with a sp^2 bonded graphitic phase is absent. Furthermore, this sample exhibited a full width at half maximum (FWHM) of the 1332 cm^{-1} Raman peak which is narrower ($\leq 5 \text{ cm}^{-1}$) than the FWHM of all other samples. It should be noted that although the zero bias conditions yielded a high quality diamond, its FWHM was not as narrow as the reverse bias sample (see Fig. 1). Also, low current reverse bias conditions ($< -60\text{V}$), which did not form a plasma, yielded diamond similar in quality to zero bias conditions but with a very low nucleation density. On the other hand, samples grown under forward or reverse bias conditions which generated a plasma contain a

significant sp^2 component) as shown in Figures 1a and 1d. Research is continuing to determine possible causes of this phenomena.

Plan view and cross sectional TEM were also utilized to examine the films grown under different biasing conditions. Figure 2 shows bright field plan-view TEM images observed with the electron beam parallel to the [011] direction revealing the defect densities of single diamond grains grown under two different biasing conditions. Under the conditions of 150V forward bias which created a DC plasma, many defects, including numerous twins, are present on the diamond grain.

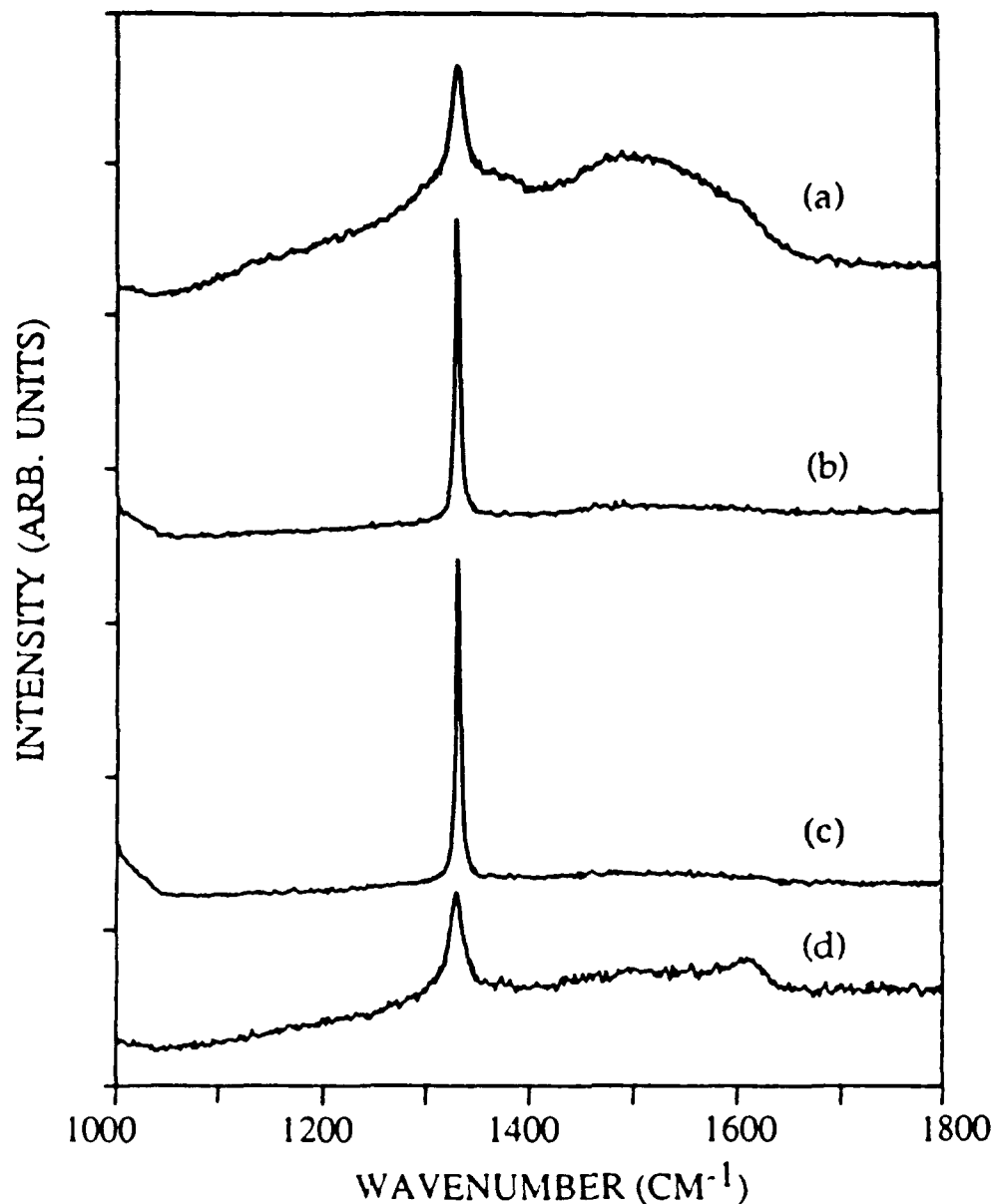


Figure 1. Raman spectra of diamond thin films grown under different biasing conditions: (a) forward bias of 150V, (b) grounded potential(0V), (c) reverse bias of 150V, (d) reverse bias of 180V. FWHM of (a) 14.0cm^{-1} , (b) 5.7cm^{-1} , (c) 5.0cm^{-1} , (d) 13.0cm^{-1} (Raman conditions: 514.5 nm Ar^+ laser, $2\text{cm} \times 2\text{mm}$ sampling area, 2cm^{-1} slit width).

In contrast, under reverse bias of 150V conditions, a much lower defect density was observed. Thus, the improved Raman characteristics correlate with a lower defect density. The corresponding bright field cross-sectional TEM micrographs are shown in Figure 3. An approximately 10 μ m thick interfacial layer as well as numerous voids were observed in the films grown under forward bias of 150 V, while no such layer was present in the film grown under reverse bias of 150V. The film grown under grounded potential has also been analyzed and exhibited similar characteristics as the 150V reverse bias film. It is believed that this is due to an increase in electron bombardment of the sample during the high forward biasing conditions which causes significant surface damage during growth.

Substrate Variations

The growth of diamond films on Si(001) and various polycrystalline metal substrates such as Ni, Mo, Ta and W has been accomplished. Films grown on Si, Ni and W exhibited the best quality according to Raman sp^2/sp^3 peak intensity ratios and the full width half maximum of the 1332 cm^{-1} Raman peak. This is discussed in more detail elsewhere [6,9]. The objective of the present research was to determine the effects of substrate surface energy on the diamond particle morphology. For heteroepitaxy of diamond thin films, it is necessary to obtain 2-dimensional or at least lateral growth. Unfortunately, this is not possible with any conventional substrate due to the high surface energy of diamond which results in a Volmer-Weber growth mechanism [10]. Therefore, an attempt was made to provide a better match of the surface free energy of the substrate to the surface free energy of diamond.

The surface free energy of diamond is estimated to be 3387 ergs/cm² [11] while the surface free energies of Si, Ni, Mo, Ta, and W are 1457 ergs/cm², 2072 ergs/cm², 2463 ergs/cm², 2628 ergs/cm², and 3111 ergs/cm², respectively [12]. Although the surface energies of the carbides of these materials are not known, their melting points increase in the same order as the surface energies of the uncarbided materials, except in the case of Si. Thus, it is not unreasonable to assume that their bond strengths and surface energies also increase in the same order.

Figure 4 shows the morphologies of diamond nuclei on substrates with different surface energies. It was observed that the aspect ratios of the diamond nuclei (i.e., the length of the nuclei parallel to the substrate versus the height of the particle perpendicular to the substrate) correlate to the surface energies for the substrates, except in the case of Si. That is, lower, flatter particles are observed on W and Ta substrates (Figures 4c and 4d) than on the Mo and Ni substrates (Figures 4a and 4b). On the Si, relatively extended lateral growth is observed which is believed to be attributed to the formation of a SiC buffer layer which will significantly affect the surface energy. Thus, changes in substrate surface energy appear to affect diamond particle profiles. Therefore, the matching of the surface free energies is an important criteria for the selection of substrate materials for the lateral, heteroepitaxial growth of diamond. It should be noted that such surface energy effects can be very sensitive to impurities and surface defects. Thus, verification of this preliminary study presented herein using carefully prepared single crystals of these same substrates is required.



Figure 2 Plan-view TEM micrographs of a diamond single grain grown under (a) forward bias of 150V (b) reverse bias of 150V

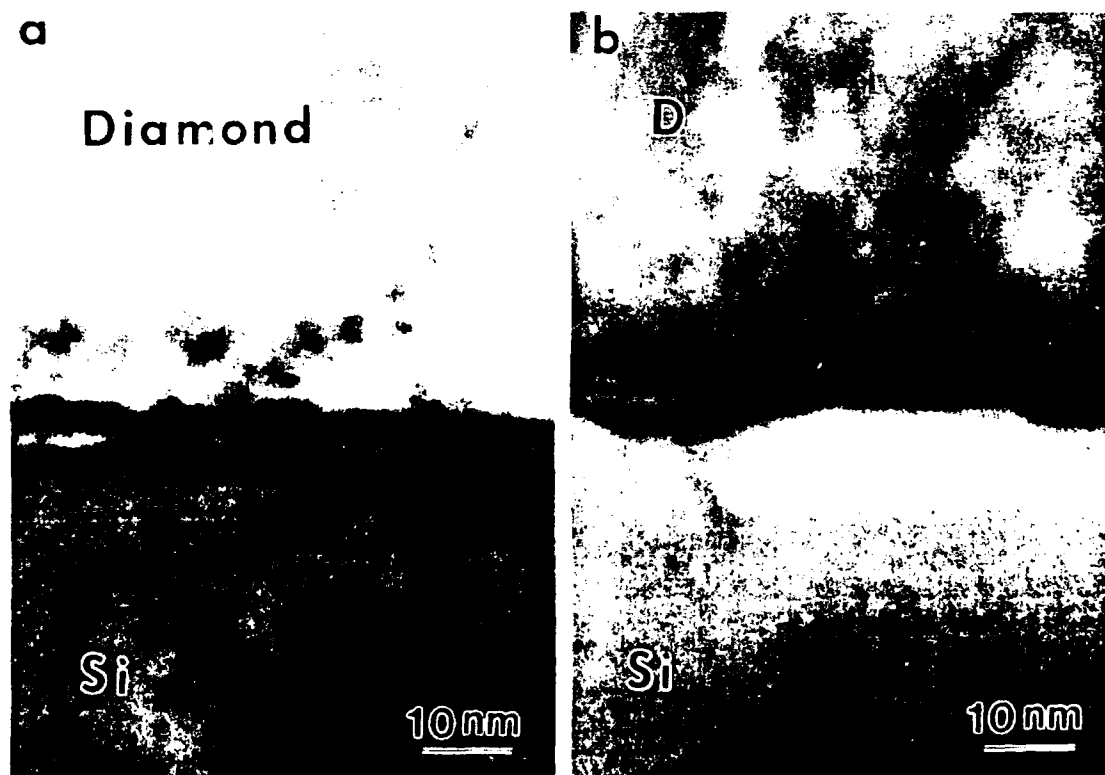


Figure 3 Cross-sectional TEM micrographs showing the interfaces between the diamond films and Si substrate grown under (a) forward bias of 150V (b) reverse bias of 150V.

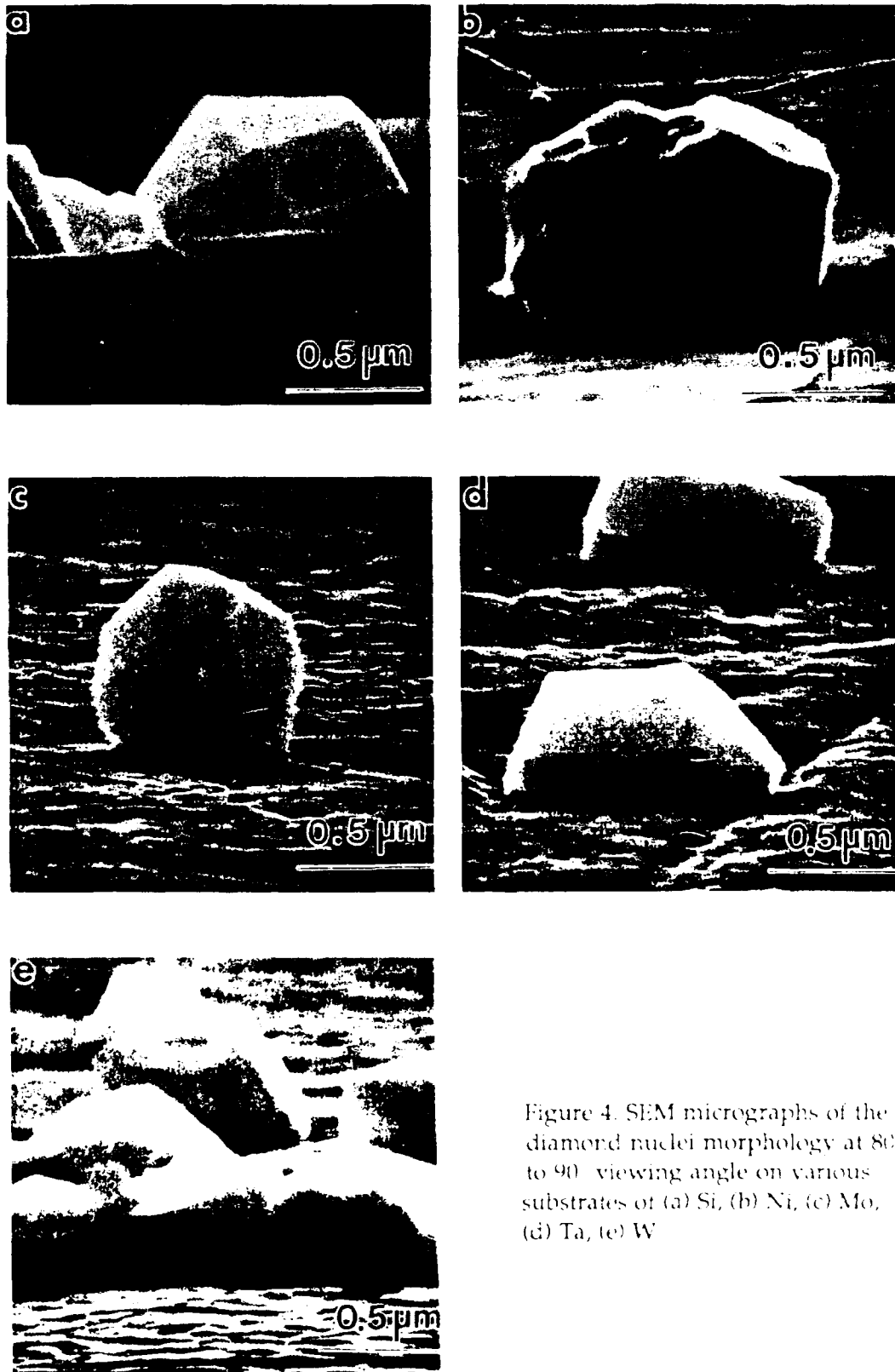


Figure 4. SEM micrographs of the diamond nuclei morphology at 80° to 90° viewing angle on various substrates of (a) Si, (b) Ni, (c) Mo, (d) Ta, (e) W

SUMMARY AND CONCLUSIONS

From the results of this research, we conclude that biasing which creates a DC plasma significantly deteriorates the film quality. In contrast, low current reverse and zero bias conditions reduce the formation of an sp^2 bonded phase and decrease the defect densities in the diamond films. Furthermore, the FWHM of the diamond Raman line was narrowest ($\leq 5 \text{ cm}^{-1}$) for the sample grown under reverse bias conditions. This is attributed to the optimization of the electron and ion bombardment of the surface which minimizes surface damage during growth. It may also be possible that the electron flux from the substrate and substrate holder surface accelerates the decomposition of H_2 into atomic hydrogen in the vicinity of the surface, and thereby suppresses the formation of the sp^2 bonded phase. It has also been shown that different substrate materials affect diamond particle morphologies. This appears to be related to the surface energy of the substrates relative to the surface energy of the diamond as is expected from crystal growth theory. Substrates which have surface energies closest to diamond yield the most extended lateral growth.

ACKNOWLEDGEMENTS

This work was supported by SDIO/IST through the Office of Naval Research (M. Yoder, contract monitor). The authors wish to thank Drs. R. F. Davis and H. S. Kong for useful technical discussions. R. J. Nemanich, Y. M. LeGrice and E. Buehler are gratefully acknowledged for obtaining the Raman spectra presented herein. Use of Field Emission SEM facilities at Research Triangle Institute (J. B. Posthill and D. P. Malta) and the assistance of S. R. Sahaida are also gratefully acknowledged.

REFERENCES

1. S. Matsumoto, Y. Sato, M. Kamo, and N. Setaka, *J. Appl. Phys.* **21**, 483 (1982).
2. M. Kamo, Y. Sato, S. Matsumoto, and N. Setaka, *J. Cryst. Growth* **62**, 642 (1983).
3. A. Sawabe and T. Inuzuka, *Appl. Phys. Lett.* **46**, 146 (1985).
4. A. Hiraki, T. Kawano, Y. Kawakami, M. Hayashi, and T. Miyasato, *Solid State Comm.* **50**, 713 (1984).
5. A. Aisenberg and R. Chabot, *J. Appl. Phys.* **42**, 2953 (1971).
6. Y. H. Lee, H. S. Kong, P. D. Richard, J. T. Glass, K. J. Bachmann, Y. M. LeGrice and R. J. Nemanich in the Summary of 4th SDIO/IST Diamond Technology Initiative Symposium, Crystal City, VA, July 1989.
7. Y. H. Lee, P. D. Richard, K. J. Bachmann, and J. T. Glass, *Appl. Phys. Lett.*, in press.
8. S. Pepper, *Appl. Phys. Lett.* **38**, 344 (1981).
9. Y. H. Lee, K. J. Bachmann, J. T. Glass, Y. M. LeGrice, R. J. Nemanich submitted to *Appl. Phys. Lett.*
10. R. Kern, G. LeLay and J. J. Metois, Basic Mechanisms in the Early Stages of Epitaxy, Current Topics in Materials Science, Volume 3, edited by E. Kaldis (North-Holland Pub. Co., 1979) p135.
11. E. D. Hondros in the Proc. TMS-AIME Heat Treatment Committee at the 1976 TMS Fall Meeting, Niagara Falls, NY, September 1976.
12. T. Takai, T. Halicioglu and W. A. Tiller, *Surf. Sci.* **164**, 341 (1985).

II. Electron microscopic characterization of diamond films grown on Si by bias-controlled chemical vapor deposition

H. M. Ma, Y. H. Lee, and J. T. Glass

Department of Materials Science and Engineering, North Carolina State University, Raleigh, North Carolina 27695

(Received 10 April 1990; accepted 19 July 1990)

Diamond films grown by Bias-Controlled Hot Filament Chemical Vapor Deposition (BCCVD) on silicon (Si) substrates were characterized by Transmission Electron Microscopy (TEM). Both plan-view and cross-sectional TEM samples were made from diamond films grown under different biasing conditions. It was found that defect densities in the films were substantially reduced under zero and reverse bias (substrate negative relative to the filament) as compared to forward bias. Furthermore, the diamond/Si interface of the reverse and zero bias films consisted of a single thin interfacial layer whereas multiple interfacial layers existed at the diamond/Si interface of films grown under forward (positive) bias. Tungsten (W) contamination was also found in the interfacial layers of forward bias films. It is concluded that forward biasing in the present condition is not favorable for growing high quality, low defect density, diamond films. The possible mechanisms which induced the microstructural differences under different biasing conditions are discussed.

I. INTRODUCTION

Diamond film and particle synthesis from the vapor phase under low pressure has been demonstrated by at least 10 different methods since it was first achieved at reasonable growth rates in 1981.¹ Currently, intensive research activities around the world are aimed at developing a new era in diamond technology which will fully utilize the unique properties of diamond in applications ranging from coatings for wear resistance and cutting tools to optical windows for visible and infrared (IR) transmission, as well as thin films for high temperature, high power semiconductor devices. A decade of research has now led in the general direction of controlling nucleation, increasing the growth rate, reducing defects, and eliminating graphite codeposition. Uniform, large area deposition, and the ultimate goal of heteroepitaxial growth of single crystal films are also major concerns of the research community.² Unfortunately, little has been known about the mechanisms of diamond nucleation and growth which would be very helpful in achieving these goals.^{3,4} Therefore, any correlation of process parameters to film properties which aids in furthering the understanding of potential nucleation and growth mechanisms is very beneficial in providing efficient guidelines for advancing the diamond technology. The present research correlates biasing conditions in a hot filament chemical vapor deposition system with film quality and defect density. This, in turn, allows speculation of the role of charged species in the mechanism of diamond growth.

Hot filament chemical vapor deposition is one of the most common diamond growth techniques due to

its simplicity and low cost.^{5,6} A heated filament above the substrate surface is utilized to thermally crack the hydrogen gas into atomic hydrogen. It also activates and dissociates the methane molecules as well as enhances surface processes via thermal excitation and electron bombardment. It has been found that placing a bias between the filament and substrate to enhance electron bombardment of the substrate has increased the nucleation density and growth rates by several times.^{7,8} This clearly implies that charged species, especially electrons, may play a significant role during the diamond growth. However, in this previous work, although growth rates and nucleation density were improved, the quality of the films was not assessed. Therefore, in the present research, a modified hot filament (or filament assisted, thermal filament) chemical vapor deposition (CVD) system is utilized to study the effects of charged species in the growth of diamond. A controlled bias is applied to the substrate and the filament independently, thus, this growth technique has been termed bias controlled CVD (BCCVD).¹¹ Transmission Electron Microscopy (TEM) was then employed to correlate the defect microstructure and the interfacial characteristics with the processing conditions. The defect densities are also compared to the surface morphologies and Raman spectra from the films.

II. EXPERIMENTAL

Diamond films were grown on silicon (001) substrates in a bias controlled hot filament chemical vapor deposition (BCCVD) system. A schematic of the growth system and its current-voltage characteristics

are presented elsewhere.¹¹ A gas mixture of methane and hydrogen in the ratio of 3%, total flow at 100 sccm, and pressure at 3.3 kPa, is introduced above a tungsten filament heated to 1930 °C. The substrate is mounted on a molybdenum holder which is heated to 850 °C by a boron nitride encapsulated heater. With all other growth parameters fixed, the filament bias and substrate bias voltage were varied independently relative to the grounded chamber. However, it was found that the current depended only on the potential difference between the filament and substrate ($\Delta V = V_{\text{substrate}} - V_{\text{filament}}$) without any influence from their position relative to ground. Films were grown under various forward bias (positive ΔV , more positive substrate potential), zero bias ($\Delta V = 0$, no potential difference), and reverse bias (negative ΔV , more negative substrate potential) conditions. TEM studies were conducted on films grown under three representative conditions, namely forward bias of 150 V ($\Delta V = 150$ V), zero bias, and reverse bias of 150 V ($\Delta V = -150$ V).

Both plan-view and cross-sectional TEM specimens were prepared with a standard ion-thinning technique. The low ion thinning rate of diamond ($\sim 0.5 \mu\text{m/h}$) and the substantial difference between the thinning rate of the diamond films and Si substrates did pose some difficulties in preparing cross-sectional TEM samples. Nevertheless, it was found that dimpling the specimens down to less than 5–10 μm of thickness (the Si appears reddish at this thickness), and then milling with Ar^+ at 6 kV, 10° incidence from both sides until perforation, then continued milling at 5 kV, 5° incidence for another hour gave very satisfactory results. The average ion milling time was approximately 6 h. The only disadvantage of this technique is that the Ar^+ tends to sputter the Mo specimen stage of the ion mill at low incident angles, and this sputtered Mo usually redeposited on the specimen surface, thereby contaminating the specimen and causing some confusion and uncertainty in the interpretation of x-ray microanalysis results. All the samples were examined either on a Hitachi H-800 scanning transmission electron microscope (STEM) operated at 200 kV, or on a Philips EM 430T transmission electron microscope (TEM) operated at 300 kV. High resolution transmission electron microscopy (HRTEM) was performed on a JEOL 200 CX TEM operated at 200 kV. Energy dispersive x-ray spectrometry (EDXS) was conducted on a Kevex ultrathin window x-ray spectrometer which is coupled with a Philips EM 430 TEM.

III. RESULTS

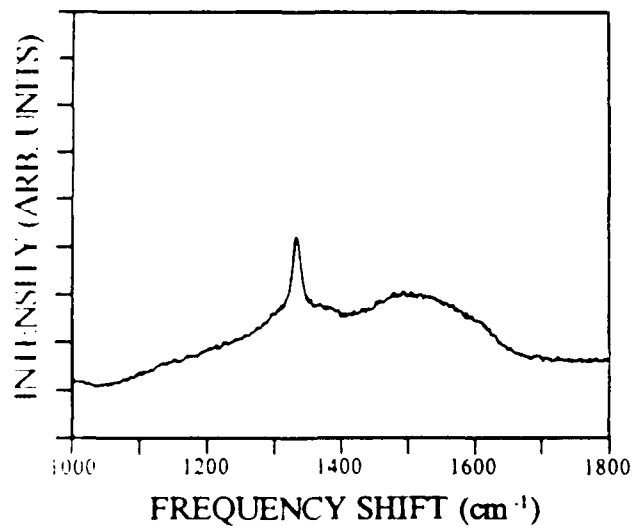
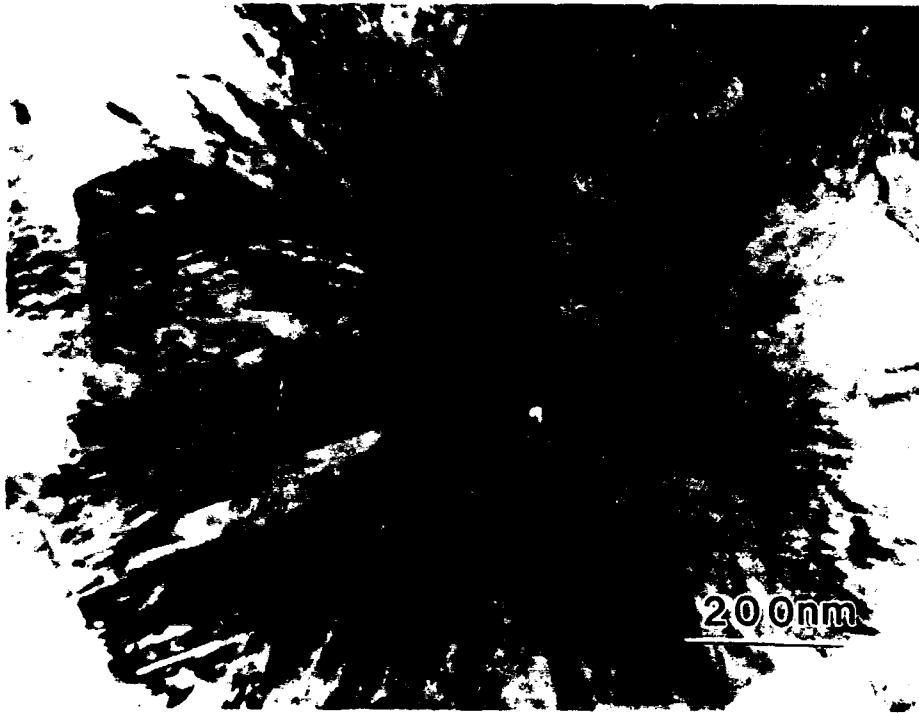
Plan-view TEM was used to investigate the defect type, density, and distribution. Figure 1 shows the plan-view TEM micrographs of diamond films grown under a forward bias of 150 V [Fig. 1(a)], zero bias [Fig. 1(b)], and reverse bias of 150 V [Fig. 1(c)] and the

corresponding surface morphology (scanning electron micrographs) and Raman spectra. For the TEM, all the individual diamond grains were tilted to the diamond $\langle 110 \rangle$ zone axis because defect density comparisons are meaningful only when compared under identical diffraction conditions. It is immediately apparent that a higher defect density is associated with the films grown under forward bias [Fig. 1(a)]. Moreover, this correlates with a degraded Raman spectrum and a poorer surface morphology (i.e., a less faceted surface). The Raman spectra can be seen to degrade in two different ways: an increase in Full Width Half Maximum (FWHM) and an increase in the intensity of the sp^2 bonded carbon peak at $\sim 1500 \text{ cm}^{-1}$ relative to the sp^3 diamond component at 1332 cm^{-1} . It is plausible that both of these changes are caused by the increased defect density (as opposed to, for example, a grain boundary phase); however, continued research is necessary to confirm such a speculation. The FWHM have been measured at 14.0 cm^{-1} , 5.7 cm^{-1} , and 5.0 cm^{-1} for forward, zero, and reverse bias diamond films, respectively, which is additional evidence of the improved quality of films grown under reverse bias. It has been shown that the FWHM is directly related to the domain size which is required for quantitative analysis of Raman spectra.¹² It was also observed that the domain sizes obtained in this method were smaller than the diamond crystal sizes observed under SEM.¹² Thus, it was speculated that the phonon scattering was confined in the local regions of the diamond crystal by defects. In the present case, using the same method as LeGrice and Nemanich,^{12,13} the domain sizes were calculated to be $\sim 51 \text{ \AA}$, $\sim 114 \text{ \AA}$, and $\sim 151 \text{ \AA}$ for forward, zero, and reverse bias films, respectively. Linear analysis was also performed on plan-view TEM micrographs to determine the defect spacing. Fifteen lines were randomly drawn across the micrographs, the number of defects (twins) were counted, and the defect spacing was obtained by dividing the total length of the lines by the total number of defects. The population of defects in forward bias films was so high that defect spacing could not accurately be obtained but appears to be less than 50 \AA . The defect spacings in zero bias and reverse bias films were found to be $\sim 710 \text{ \AA}$ and $\sim 750 \text{ \AA}$, respectively. These values are higher than the domain sizes obtained from the FWHM. However, as shown in Figs. 1(b) and 1(c), the defects are not distributed evenly in the films; thus, the FWHM could be affected by local high defect density regions (such as near the grain boundaries), yielding a smaller domain size. Qualitatively, the defect spacing seems to correspond to the domain size. However, an exact relationship between domain size and defect spacing could not be drawn here, since a larger data base is needed to make this correlation statistically meaningful. Regardless, both parameters indicate the

poor quality of the forward bias films and imply that the reverse bias films may be of slightly higher quality than those grown at zero bias.

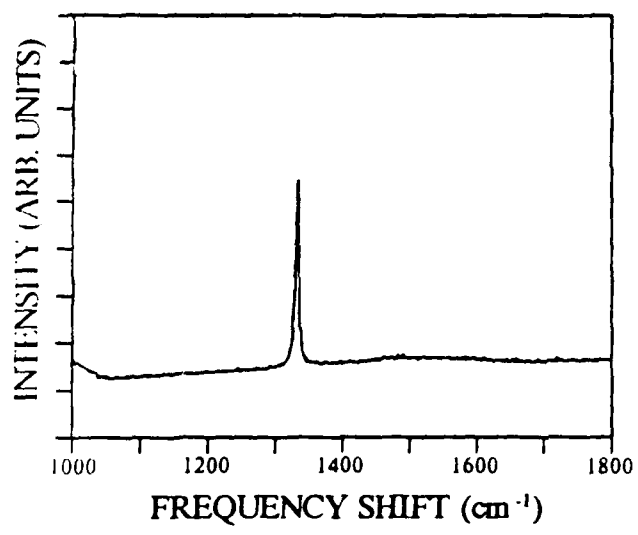
It is also observed that the numerous defects emerge from the center of an individual diamond grain grown under forward bias, as shown in Fig. 1(a). Closer

examination shows that those defects are twins and microtwins. Twinning in $\{111\}$ has been known to be the predominant defect in CVD diamond.^{14,15} The grain in Fig. 1(a) is also "multiply twinned" with five-fold symmetry apparent at the center of the grain. Such fivefold multiply twinned particles (MTP) are com-



(a)

FIG. 1. Plan view TEM micrographs of a single diamond grain grown under (a) forward bias of 150 V, (b) zero bias, (c) reverse bias of 150 V, and corresponding scanning electron micrographs and Raman spectra of diamond films.

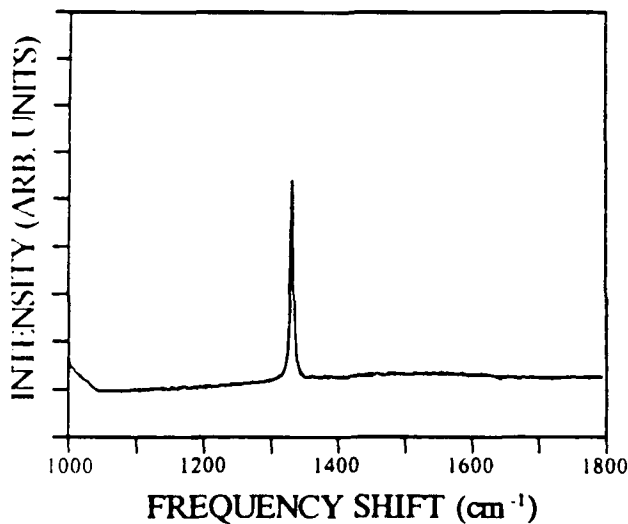
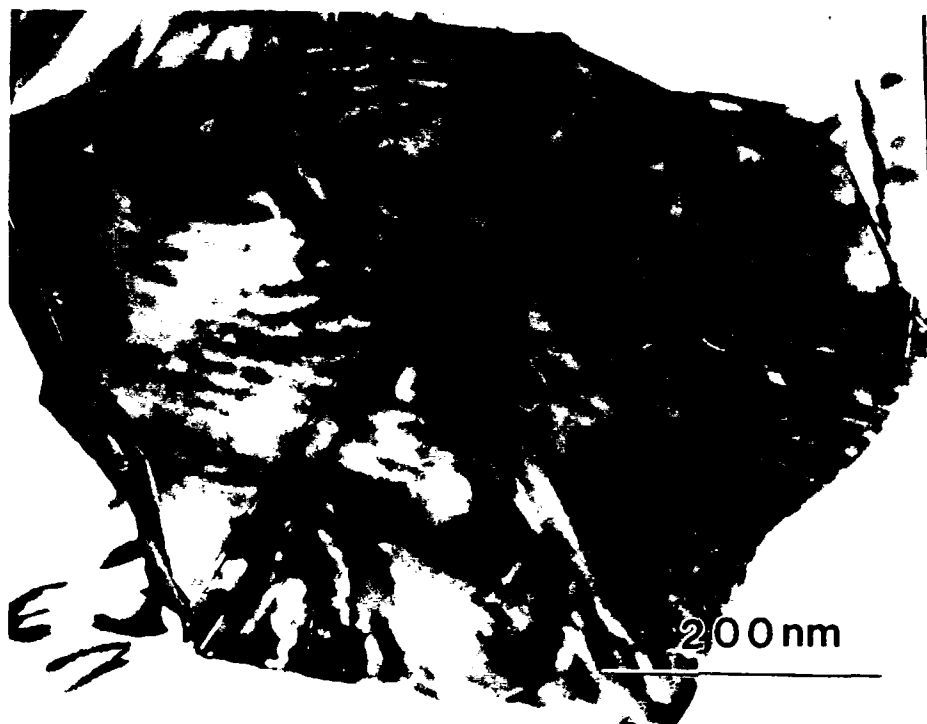


(b)

FIG 1 (continued)

monly seen in plasma enhanced CVD diamond and have been studied thoroughly.^{16,17} No other type of defect was apparent; however, due to the indistinguishable nature of simple stacking faults versus microtwins whose thicknesses are a few tens of Å,¹⁸ some stacking faults may also exist. In the zero and reverse bias films [Figs. 1(b) and 1(c)], the density of defects (i.e., the

number of twin plates) is seen to be reduced significantly. Selected area diffraction (SAD) indicated again that the twinning occurred along {111}. There was no major difference between the defect density of the zero and reverse bias films, although, as stated earlier, spacings were somewhat larger in the reverse bias films. The defects emerge from the center of the diamond



(c)

FIG 1 (continued)

grain to the grain boundary, but are not distributed evenly.

Cross-sectional TEM (XTEM) micrographs of diamond films grown under a forward bias of 150 V, zero bias, and reverse bias of 150 V are shown in Figs. 2(a), 2(b), and 2(c), respectively. It is noted that in all the

micrographs the defects (dark lines and zones) emerge from the center of the base of each crystal. This is similar to previous observations in diamond films grown by plasma assisted CVD methods.¹⁹⁻²¹ Since the defects are generated because of the growth species sitting in the improper lattice sites during the deposition process,

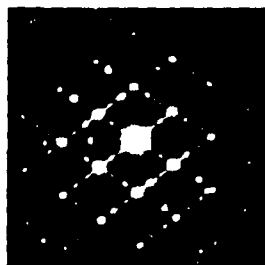
the defect lines actually reflect the trace of crystal growth.¹⁹ Thus, this implies that each diamond grain is nucleated from the single site from where the defects nucleated and undergoes a three-dimensional growth. The similar growth morphologies in films grown by different techniques suggest that, in some respects, similar growth mechanisms exist regardless of the diamond growth techniques used.

The forward bias films consist of several fan-shaped sectors which are full of defects (dark lines), as shown in Fig. 2(a). The SAD pattern over the entire grain shows a single crystal (110) spot pattern with intensive twin spots [Fig. 2(a) inset]. This pattern suggests that those fan-shaped sectors (subgrains) are

actually twin-related and the "grains" are due to multiple twinning. This observation correlates very well with SEM observations. In the zero bias films, as shown in Fig. 2(b), only a few dark lines emerging from the center of the grain are present, indicating the defect density has been substantially reduced. Well-defined grain outlines show the (111) plane at the surface which correspond to the highly faceted morphology observed in the SEM. The variation in contrast inside the diamond grain and the SAD pattern confirmed the grain is also multiply twinned but with fewer twin sectors (subgrains). XTEM of the reverse bias diamond films [Fig. 2(c)] also showed a well-faceted crystal surface and a low defect similar to the zero bias films.



(a)



(b)



(c)

Fig. 2. Cross-sectional TEM micrographs showing the growth morphology of diamond crystals grown under a forward bias of 150 V (a), zero bias (b), and a reverse bias of 150 V (c).

XTEM was also used to reveal differences in the characteristics of the diamond/Si interface under different biasing conditions. All the specimens were tilted to the Si [110] pole for edge-on viewing. Figures 3(a)–3(c) reveal the diamond/Si interfacial area and the corresponding electron diffraction patterns under different biasing conditions. It is obvious that in the forward bias condition, the interface consists of multiple structures over rather extended regions (~ 200 Å), as shown in Fig. 3(a). It appears that a region of foreign particles is deposited first, followed by a thin layer of film, and finally another region of apparent particulates before the growth of the diamond. In contrast, XTEM micrographs in Figs. 3(b) and 3(c) showed that only a single thin interfacial layer is present in films grown under zero bias and a reverse bias of 150 V. Its thickness varies between 20 Å and 40 Å, depending on surface roughness. The diffraction patterns also confirm that multiple phases exist in the forward bias film, while only Si and diamond (pointed by arrows) spots are observed in the zero and reverse bias films. These interfacial structures have been investigated further by

HRTEM. Figure 4 shows an HRTEM micrograph of a reverse bias film; the atomic fringes of Si and lattice fringes of diamond are clearly seen. No attempts were made to determine the exact atomic positions at the interface as this involves detailed defocusing experiments and extensive image simulations which are beyond the scope of the present manuscript. However, the lattice spacing of the interfacial layer is very close to Si and it is closely aligned with the Si substrate. In addition, no diffraction spots appear in the SAD pattern other than spots from Si and diamond (Fig. 4). It can be speculated that this interfacial layer might be Si damaged during substrate pretreatment (scratching), and then recrystallized in the initial stages of diamond growth when the substrate temperature is raised. However, more detailed HRTEM is needed to confirm this theory.

Energy dispersive x-ray spectrometry (EDXS) was used to characterize the chemistry of the interfacial layers of all the films studied in the TEM. An electron probe with a diameter of ~ 100 Å is focused onto the diamond/Si interface and x-ray spectra were collected

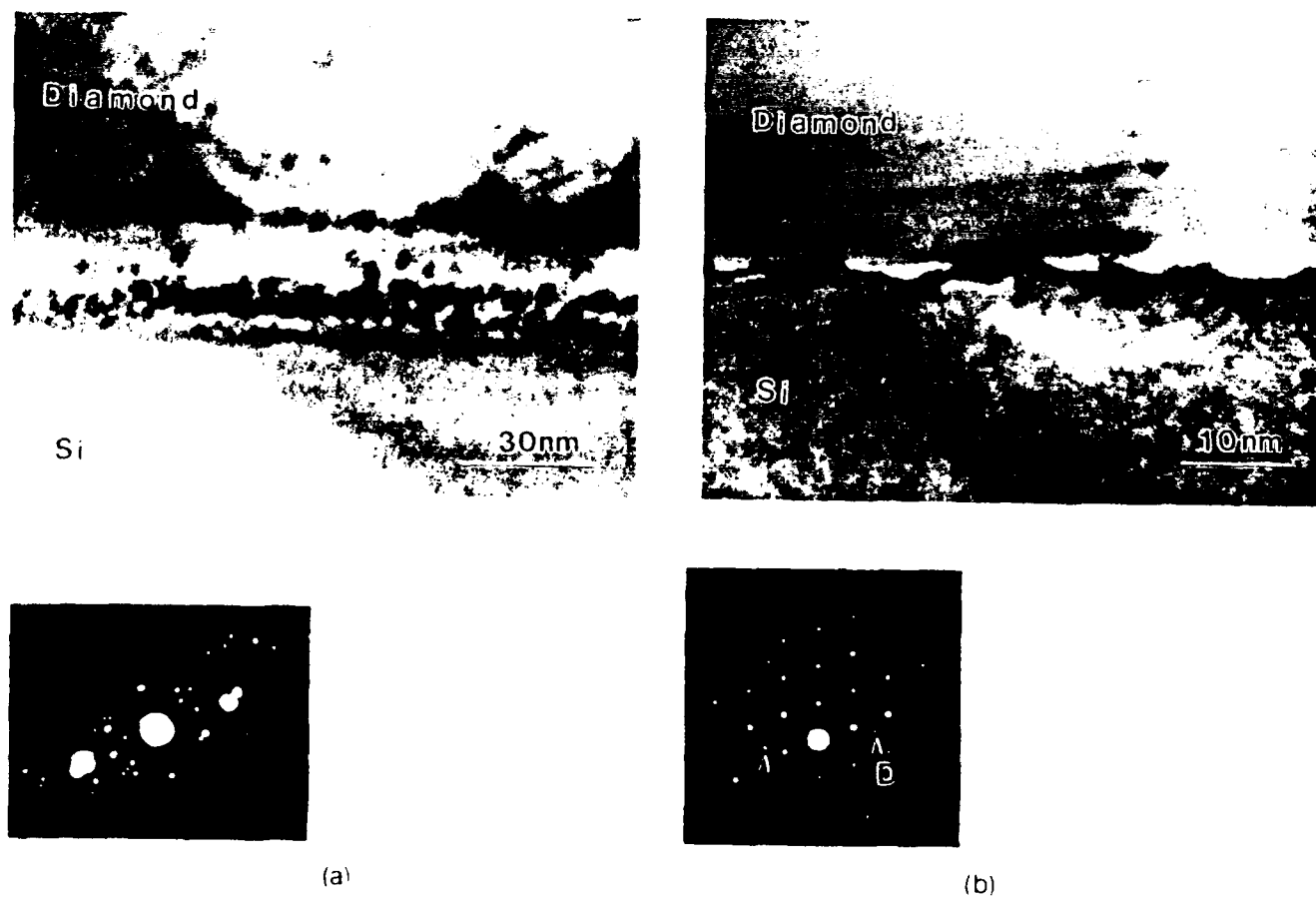
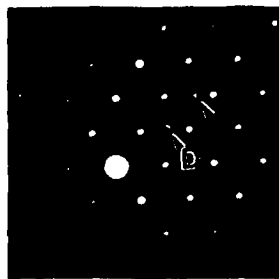
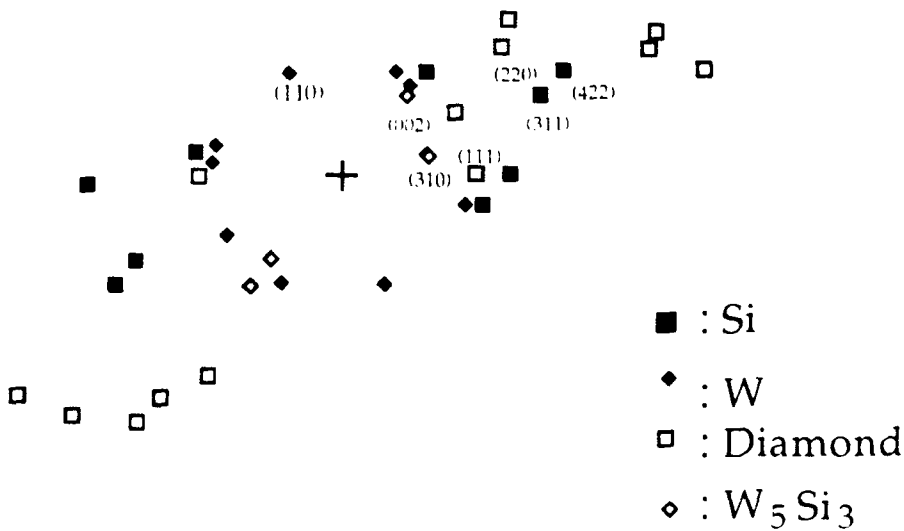


FIG. 3. Cross-sectional TEM micrographs and corresponding SAD patterns showing diamond/Si interfacial structure of diamond films grown under (a) forward bias of 150 V, (b) zero bias, and (c) reverse bias of 150 V. (d) Indexing of SAD pattern of forward bias film [shown in (a)] reveals multiple phases in the interfacial region.



(c)

FIG. 3. (continued)



(d)

for 300 s. These spectra indicated the presence of Si, molybdenum (Mo), and tungsten (W) in forward bias interfacial layers, as shown in Fig. 5, while only Si and Mo show up in the spectra collected from interfacial layers formed under reverse bias and zero bias. It is believed that the Si is from the substrate and that the Mo

is a contaminant from sample preparation (ion milling). Mo is found in all TEM samples prepared with the technique described in the experimental section, but is not observed in samples prior to ion milling. Hole count spectra (i.e., spectra taken while the electron beam was focused through the hole in the TEM sample) were also

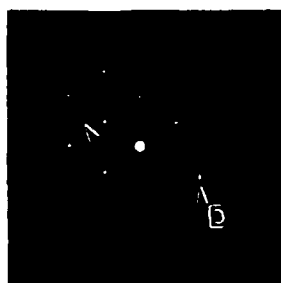
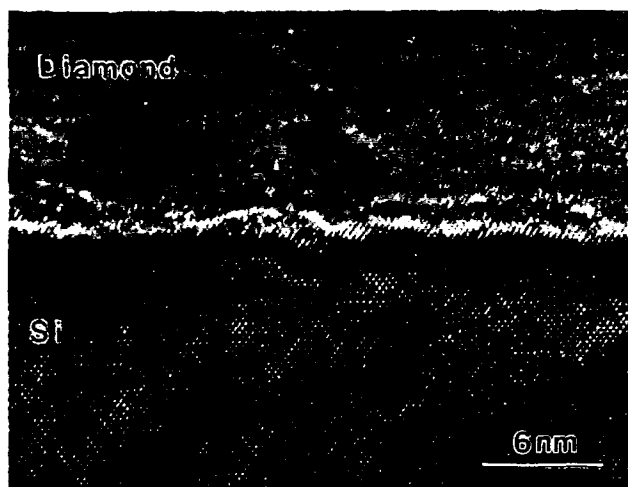


FIG. 4 High resolution TEM micrograph showing the detailed diamond interfacial structure of reverse bias films.

taken and showed only traces of Si. This verifies that the data collected were not an artifact of extraneous signals from beyond the sample. Spectra were also collected inside the Si and diamond near the interface area; no W was found in either of those spectra within the detectability limit of this technique (~ 0.1 wt. %). Therefore, the possibilities of this W contamination from the microscope or sample preparation were care-

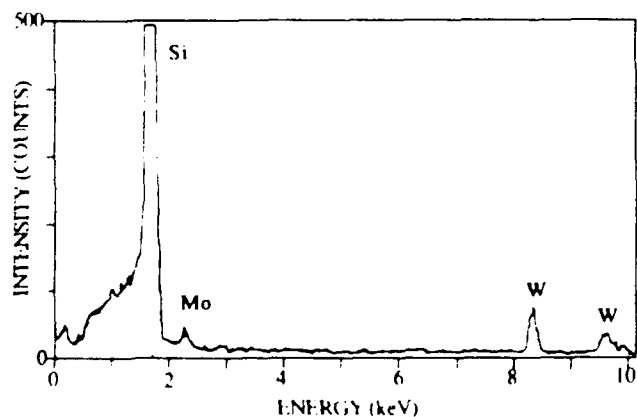


FIG. 5 Energy dispersive X-ray spectrum taken from interfacial area of 150 V forward biased films showing the presence of tungsten (W, L_{23} = 8.396 KeV, L_{23} = 9.67 KeV).

fully eliminated. Consequently, the source of this W contaminant is believed to be the tungsten filament used inside the growth chamber, probably caused by the dc plasma created via forward biasing. This biasing attracts positive species to the filament, which sputter W into the gas which then redeposits on the substrate. Additionally, from electron microdiffraction results, it appears that no tungsten carbide phases exist at these tungsten contaminated interfacial layers within the detectability of the microscope. However, diffraction spots with their lattice spacing very close to elemental tungsten and tungsten silicide (W_3Si_2) were observed [Fig. 3(d), SAD pattern indexing].

IV. DISCUSSION

From the present results, it has been shown that biasing affects film microstructures. Thus, charged species (ions and electrons) under different biasing conditions have strong influences on the diamond growth mechanism(s). To elucidate the roles of charged species in affecting diamond growth, the possible sources of such species have to be discussed. Generally, in the current system, there are three possible sources for charged species: (1) thermionic emission of electrons from the filament, (2) surface ionization of the gas atoms or molecules when they impinge onto the heated filament and substrate holder surfaces, and (3) impact ionization when particles (electron, ion, or neutral atoms) collide with each other and kinetic energy is exchanged. From a comparison of the experimental I-V characteristics with theoretical calculations of current expected from these mechanisms, it can be concluded that the possible dominant conduction mechanisms (charged species generated current conduction) are impact ionization for the reverse bias condition, while thermionic emission and impact ionization are the dominant mechanisms under forward bias conditions.²² The major charged species on the growth surface under forward bias are believed to be electrons, while under reverse bias the major charged species on the growth surface are positive ions. However, since not any single mechanism can explain the current phenomena clearly by itself, it is very possible that two or even three of the mechanisms occur at the same time. The quantitative participation of each mechanism in the growth is not known and would be very difficult to verify experimentally. Please refer to Ref. 22 for more detailed discussions of these mechanisms.

Since no gas phase analysis was performed in the present system, it would be premature to speculate as to what type of ions is actually present. However, Celi *et al.*²¹ and Harris and Weiner²⁴ have measured the stable gas phase species present in the hot filament assisted CVD system with similar gas inputs (hydrogen and methane). Celi *et al.*²¹ concluded that methyl

(CH₃), acetylene (C₂H₂), and ethylene (C₂H₄) were detected above the growing surface, while Harris and Weiner²⁴ concluded that diamond growth occurs mainly from reactions involving acetylene, ethylene, methane, and/or methyl radicals. It could be envisioned that similar species exist in the present system, and the possible ionization processes of these species are likely to be important. However, continued research is necessary for a thorough understanding of this speculation and is beyond the scope of the current research.

Under forward bias conditions, the substrate is positive relative to the filament, and the electrons are the dominant charged species near the growth surface. It was observed that higher currents were generated under forward bias than in reverse bias with the same voltage.²² This implies that a higher flux of charged species (electrons) impinges onto the substrate surface under forward bias conditions. Since the electrons strike the surface with a finite energy caused by the potential difference between the filament and substrate, they could very possibly damage the growth surface and alter the surface energy. In this regard, it is worthwhile to point out that hydrogen desorbs from the diamond surface at approximately 900 °C, causing surface reconstruction.^{25,26} This reconstruction creates π , double bonded surface states which are not conducive to the growth of high quality diamond. The current growth temperature (850 °C) is very close to this transformation temperature, presumably to allow activation of the surface hydrogen for enhanced exchange with the incoming carbon while at the same time avoiding reconstruction. Thus, the additional energy supplied by the incident electrons attracted to the surface by the forward biasing may be sufficient to desorb the hydrogen, causing local regions of surface reconstruction or 'defective bonding', leading to line and planar defects. This is even more plausible when one considers that a twin boundary requires only a 60° rotation of the surface bonding [assuming growth takes place on the diamond (111) plane]. It is a relatively low energy modification of the original surface and thus could be considered to be caused easily by an incident flux of electrons. This is supported by the prevalence of twins in these films. On the other hand, the lower flux of charged ions under reverse bias (as observed by the much lower currents) will not cause as much surface modification and thus results in fewer twins.

V. CONCLUSIONS

In summary, the defect density of diamond films grown under forward bias conditions was much higher than those of zero bias and reverse bias. This increased defect density correlated with an increase in the FWHM of the Raman diamond line as well as an increase in the sp^2/sp^1 peak intensity ratio. Furthermore,

the interfacial area of the forward bias films was found to be contaminated with tungsten. It was also found that the microstructures of the films grown under zero and reverse bias are very similar, although the defect density and Raman FWHM imply that the reverse bias films may be somewhat better quality. It should be noted that recent results currently in preparation for publication also indicate reduced contamination in the reverse bias films, not observable in TEM. From these results, it is clear that the biasing condition, which influences the role of charged species in the growth of diamond, affects the defect density and the nature of the diamond/substrate interface. Under forward bias which creates a dc plasma, more electrons and other negatively charged radicals are attracted by the more positive substrate. Those negative species might either bombard the substrate surface, creating surface damage and/or changing the nature of the hydrogen desorption reaction which occurs during diamond growth, or they may interact with hydrogen and methane in the gas phase. Moreover, the tungsten filament used in the growth chamber is eroded by the dc plasma and creates a large population of W in the gas phase which later redeposits on the surface of the substrate. In all these cases, the surface energy and/or chemistry (surface or gas phase) were altered, creating conditions which are not favorable for high quality, low defect density diamond growth on Si.

ACKNOWLEDGMENTS

This work was supported in part by SDIO/IST through the ONR under contract No. N00014-86-K-0666. Use of TEM facilities at Microelectronics Center of North Carolina (MCNC) and the assistance of Dr. S. Chevacharoenkul is gratefully acknowledged. Appreciation is extended to Dr. R. F. Davis for the use of his facilities. The authors would also like to thank Dr. R. J. Nemanich, E. C. Beuhler, and Y. M. LeGrice for the Raman spectra presented, and S. Sahaida for his assistance in diamond growth.

REFERENCES

- ¹B. V. Spitsyn, L. L. Bouilov, and B. V. Deryagin, *J. Cryst. Growth* **52**, 219 (1981).
- ²Karl E. Spear, *J. Am. Ceram. Soc.* **72** (2), 171 (1989).
- ³M. Tsuda, M. Nakajima, and S. Oikawa, *J. Am. Chem. Soc.* **108**, 5780 (1986).
- ⁴M. Frenklach and K. E. Spear, *J. Mater. Res.* **3**, 133 (1988).
- ⁵S. Matsumoto, Y. Sato, M. Tsutsami, and N. Setaka, *J. Mater. Sci.* **17**, 3106 (1982).
- ⁶S. Matsumoto, Y. Sato, M. Kamo, and N. Setaka, *J. Appl. Phys.* **21**, 483 (1982).
- ⁷Y. Hirose and Y. Terasawa, *Jpn. J. Appl. Phys.* **25**, L519 (1986).
- ⁸B. Singh, Y. Arie, A. W. Levine, and O. R. Mesker, *Appl. Phys. Lett.* **52** (20), 1658 (1988).
- ⁹A. Sawabe and T. Inuzuka, *Appl. Phys. Lett.* **46**, 146 (1985).
- ¹⁰A. Sawabe and T. Inuzuka, *Thin Solid Films* **137**, 89 (1986).

- ¹¹Y. H. Lee, P. D. Richard, K. J. Bachmann, and J.T. Glass, *Appl. Phys. Lett.* **56** (7), 620 (1990).
- ¹²Y. M. LeGrice, M.S. Thesis, North Carolina State University (1990).
- ¹³Y. M. LeGrice and R. J. Nemanich, in *Diamond, Boron Nitride, Silicon Carbide and Related Wide Bandgap Semiconductors*, edited by J.T. Glass, R. F. Messier, and N. Fujimori (Mater. Res. Soc. Symp. Proc. **162**, Pittsburgh, PA, 1990).
- ¹⁴S. Matsumoto and Y. Matsui, *J. Mater. Sci.* **18**, 1785 (1983).
- ¹⁵W. Zhu, A. B. Badzian, and R. Messier, *J. Mater. Res.* **4**, 659 (1989).
- ¹⁶B. E. Williams, H. S. Kong, and J.T. Glass, *J. Mater. Res.* **5**, 801 (1990).
- ¹⁷J. Narayan, A. R. Srivatsa, and K.V. Ravi, *Appl. Phys. Lett.* **54** (17), 1659 (1989).
- ¹⁸G. S. Woods, *Philos. Mag.* **23**, 473 (1971).
- ¹⁹H. Kawarada, K. S. Mar, J-I. Suzuki, T. Ito, H. Mori, H. Fujita, and A. Hiraki, *Jpn. J. Appl. Phys.* **26** (11), L1903 (1987).
- ²⁰J-S. Ma, H. Kawarada, T. Yonehara, J-I. Suzuki, J. Wei, Y. Yokota, H. Mori, H. Fujita, and A. Hiraki, *Appl. Surf. Sci.* **41/42**, 572 (1989).
- ²¹B. E. Williams and J.T. Glass, *J. Mater. Res.* **4**, 373 (1989).
- ²²Y. H. Lee, Doctorate Dissertation, North Carolina State University (1990).
- ²³F. G. Celii, P. E. Pehrsson, H-T. Wang, and J. E. Butler, *Appl. Phys. Lett.* **52** (24), 2043 (1988).
- ²⁴S. J. Harris and A. M. Weiner, *Appl. Phys. Lett.* **53** (17), 1605 (1988).
- ²⁵S. V. Pepper, *J. Vac. Sci. Technol.* **20** (2), 213 (1982).
- ²⁶S. V. Pepper, *Appl. Phys. Lett.* **38** (5), 344 (1981).

III. Novel Approaches to the Attainment of the Heteroepitaxy of Diamond Films

A. Overview

The goal of this study is to achieve epitaxial growth of single crystal diamond films on one or more nondiamond substrates. The resulting film can be extremely thin - e.g., 50 - 500Å; since, it will be used as a template on which to grow thicker diamond films by a more conventional process such as plasma CVD. The techniques given below may be divided into four groups: (a) high pressure, (b) ion beam enhanced epitaxy, (c) carbon ion implantation into copper, and (d) the use of surfactants.

B. The Use of the Pressure Variable for the Conversion of Amorphous "Diamond"

The objective of this approach is to form monocrystalline diamond films by producing thin, H-free diamond-like C films on suitable substrates followed by exposure of the assemblies to sufficient pressure and temperature to cause crystallization to diamond. The reasoning which supports this approach follows both from the enhanced crystallization and diffusion rates produced by the negative (assumed) activation volume and the driving force of epitaxial relationships. It may be necessary (or at least helpful) to use epitaxy to cause the formation of diamond, if we can get the film to crystallize from the substrate to the film surface rather than vice-versa which is the more common case. The initial substrates will be Diamond(110), Si(100) and β -SiC(100). The biggest concern of ours in conducting this study is to be able to apply pressure to the diamond-like amorphous C film and to simultaneously monitor any structural changes in the film, especially the nature of the bonding.

Dr. David Schefferal of Los Alamos National Laboratory has a high-pressure diamond anvil cell containing a window for *in-situ* Raman spectroscopy. He has agreed to collaborate with us on this program. Raman spectroscopy will provide a continuous stream of information regarding the structure and bonding of the material as a function of applied pressure and temperature. Since the pressure cell contains diamond the laser beam for the Raman analysis will have to be focused such that only the film is in the focal plane. This is made possible by a

technique called Confocal Micro-Raman Spectroscopy, which incorporates an additional lens into the optics to focus the laser beam into a finer probe size. The pressure is measured using a very small ruby crystal that is placed near the sample. Fortunately, we have a similar but lower temperature and pressure apparatus in the physics department at NCSU which is under the supervision of Dr. Michael Paesler. Dr. Paesler and his student (Gerd Pfeiffer) have agreed to assist us in the preparation of the samples.

The upper limits of the high-pressure diamond anvil cell at Los Alamos are as follows:

Maximum Pressure = 200 kbar

Maximum Temperature = 900°C (long term use @ 700°C)

Maximum sample dimensions = 0.1mm X 0.1mm X 0.1mm

Pressure medium = cryogenic argon.

Cryogenic argon (80K) is used as a pressure medium to insure that the applied pressure is homogeneously distributed across the surface. It also provides an inert atmosphere to minimize sample contamination.

H-free amorphous carbon films are desired because, if present, H ties up dangling C bonds which would preferably become sp^3 under selected pressure/temperature regimes. A method called Elastic Recoil Detection (ERD) will be used to measure the H content in the diamond-like C films. (This method is described in more detail by: H.C. Hofsass, et al, Nuclear Instruments and Methods in Physics Research B45, pp. 151-156 (1990)). ERD is a highly sensitive technique for detecting light elements in thin samples containing heavier elements. In this technique MeV He^+ ions are incident on a thin target and the energies of both the forward-scattered He ions and the elastically recoiled light atoms are detected in coincidence. Concentration-versus-depth profiles can be obtained from the measured number of coincidence events for a depth range of $1\mu m$ and for all recoiled light elements.

Dr. Bruce Sartwell at the Naval Research Laboratory in Washington D.C. has agreed to characterize the diamond-like C films for H content using ERD. The amount of sp^3 bonding in the film also needs to be determined prior to the application of pressure. Dr. James E.

Butler at the Naval Research Laboratory, Chemistry Division will analyze the bonding nature of the film using Raman Spectroscopy .

Samples of sputtered films have been sent to the Naval Research Laboratory for H-content and sp^2/sp^3 analysis, and the results should be forthcoming. The diamond-like C films were prepared using rf sputtering. A 5-inch diameter pyrolytic graphite target attached to the cathode was the carbon source. Silicon was used as the substrate. The chamber was pumped to 10^{-6} torr before introducing high purity argon as the sputtering gas. During sputtering, the argon pressure was maintained at 10 mtorr. No hydrogen was intentionally admitted into the chamber. A plasma of Ar ions and electrons was formed using the rf power supply (50, 100 & 200 watts). The pyrolytic graphite target was presputtered at 300 watts for 30 minutes to enhance the sputtering efficiency by removing any impurities present at the target surface. All of these sputtering experiments were performed at room temperature.

C. Ion Beam Enhanced Epitaxy (IBEE) of Diamond and Amorphous-C Films

In this study, a (100) diamond crystal will be ion implanted (@ 77K) using a C ion beam having sufficient energy and dosage to amorphize the surface layer. The temperature and energy of the second C implant will be raised to cause solid phase epitaxy (SPE) of the amorphized layer. The amorphized layer must be thin in order to achieve epitaxy completely to the surface. The beauty of this technique is that the recrystallization begins at the substrate/amorphized layer interface rather than at the surface.

Alternatively, an amorphous carbon film will be deposited on (100) diamond and on other substrates such as (100) and (0001) SiC, polycrystalline cBN and (100) Ni. Subsequently, high energy C ion implantation will be conducted to cause SPE on the selected substrates. Dr. Stephen Withrow of Oak Ridge National Laboratories in Knoxville, Tennessee has agreed to work with us on the ion implantation of the samples. The parameters which influence the regrowth rate, such as dose rate, target, target temperature, ion species, and ion energies will have to be optimized. Listed are preliminary estimates for these parameters:

<u>Targets</u>	<u>Ion Species</u>	<u>Temperature</u>	<u>Energies(keV)</u>	<u>Dose Rate (ions/cm²)</u>
(100) Diamond	C	77K	150-225	1.5 - 5.0 x 10 ¹⁵
Amorphous Diamond	C	300-500°C	250-350	10 ¹⁶ - 10 ¹⁷
Amorphous C	C	300-500°C	250-350	10 ¹⁶ - 10 ¹⁷

D. Carbon Ion Implantation of Copper

Background. Prins et. al. (presentation at the Diamond Conference in Washington D.C., Sept. 1990) recently reported that epitaxial diamond layers can be grown on single crystal (111) copper by means of high dose carbon ion implantation at elevated temperatures. Copper has a lattice constant close to diamond and has a very low solid solubility of carbon under the implantation conditions. At elevated temperatures, the implanted carbon atoms diffuse to the surface, due to thermal activation and the lack of solubility in copper, and they arrange themselves, under the influence of the host copper material, to the diamond lattice. Once a thin film of diamond is formed in this manner a thicker film can be achieved by using it as a template.

Experimental. A similar experiment to that of Prins was carried out at NCSU to verify the existence of a diamond film on (100) copper. Copper substrates, 99.999% pure with a diameter of 0.5 inches and a thickness of 1.75mm, were electropolished and cleaned prior to this experiment. The implantations were carried out using ¹²C species, obtained from a CO₂ gas source, at a substrate temperature of 900°C with the following ion doses and energies:

- (1) 5 X 10¹⁷ions/cm² @ 120keV and a beam angle of 0°
- (2) 1 X 10¹⁸ions/cm² @ 150keV and a beam angle of 10°.

The implanted samples were characterized using Auger Electron Spectroscopy (AES), Secondary Ion Mass Spectroscopy (SIMS), and Scanning Electron Microscopy (SEM).

Results & Discussion. *Surface Morphology.* Scanning electron microscopy was used to study the surface morphology of the ion implanted copper substrates. The samples implanted with 5 X 10¹⁷ions/cm² @ 120keV and a beam angle of 0° (sample 1 & 2) did not

exhibit much of a surface structure. The only noticeable features were long scratches caused by the polishing procedure, as illustrated by Fig. 1(a-c). Fig. 1c shows a surface phase residing on and along the sides of the scratch. The width of the scratch is approximately $1\mu\text{m}$. Also, Fig. 1c shows a large number of dark spots, which could not be resolved at higher magnification. The origin of these spots is not known at this time.

The samples implanted at 150keV with a dose of $1 \times 10^{18}\text{ions/cm}^2$ and a beam angle of 10° (sample 3 & 4) exhibited a plethora of surface detail but had different surface morphologies. Sample 3 appeared to have a network of globules, approximately $1\mu\text{m}$ wide, resting on the surface which is covered by 100nm size particles, as shown in Fig. 2(a-c). Fig. 2c shows a close-up view of one of the large globules which could have grown as a result of the smaller particles clustering together. Another point to note is the irregular shape of the smaller particles, whereas, the larger particle appears smoother. Sample 4 which was implanted under the same conditions as sample 3 is shown in Fig. 3(a-c). As illustrated in Fig. 3a, this sample has a different surface morphology as compared with sample 3, shown in Fig. 2. On first glance, this sample appears to have "caves" (a few μm in diameter) which are filled with irregularly shaped particles approximately 100nm in diameter. But, a closer look at the regions between the "caves" reveals a smooth, glassy phase similar to the globules of Fig. 2. Based upon a comparison of the micrographs in Figures 2 & 3 it can be inferred that the only difference in the two samples is that the globules in Fig. 3 had a chance to grow until they started to attach to each other. Fig. 2a shows that the globules are not symmetrical in geometry, rather they tend to be longer in one direction. Because of this asymmetry these globules tend to be connected in the length-wise direction rather than along their width. Thus, the regions between the globules remain uncovered and form what appears to be a cave-like structure, as illustrated in Fig. 3. These caves have particles inside with the same irregular shape and size as the 100nm particles in Fig. 2. Samples 3 & 4 are, therefore, very similar in morphology with the only difference being the size of the globules.

(a)



(b)

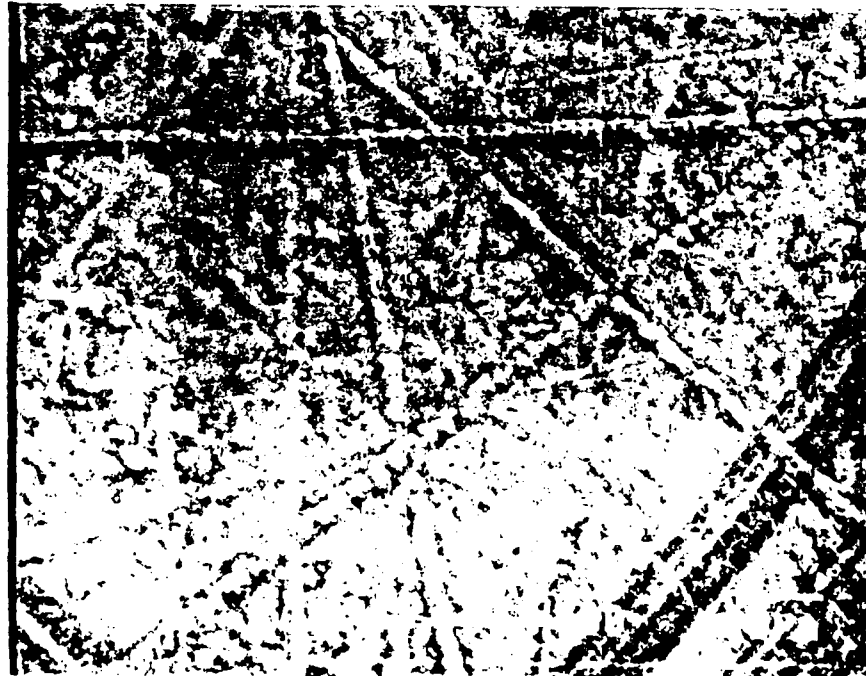


Figure 1. Cu samples implanted with a dose of 5×10^{17} ions/cm², an energy of 120keV and a beam angle of 0° (samples 1&2). Note the long scratches probably caused by the polishing procedure.

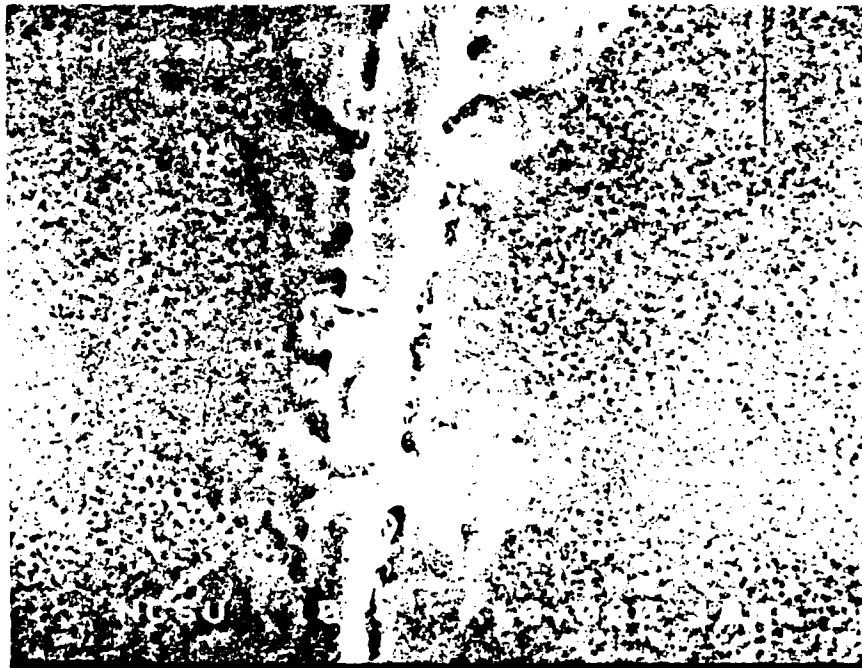


Figure 1(c). An amorphous phase residing on the scratch. The width of the scratch is approximately $1\mu\text{m}$.

(a)



(b)

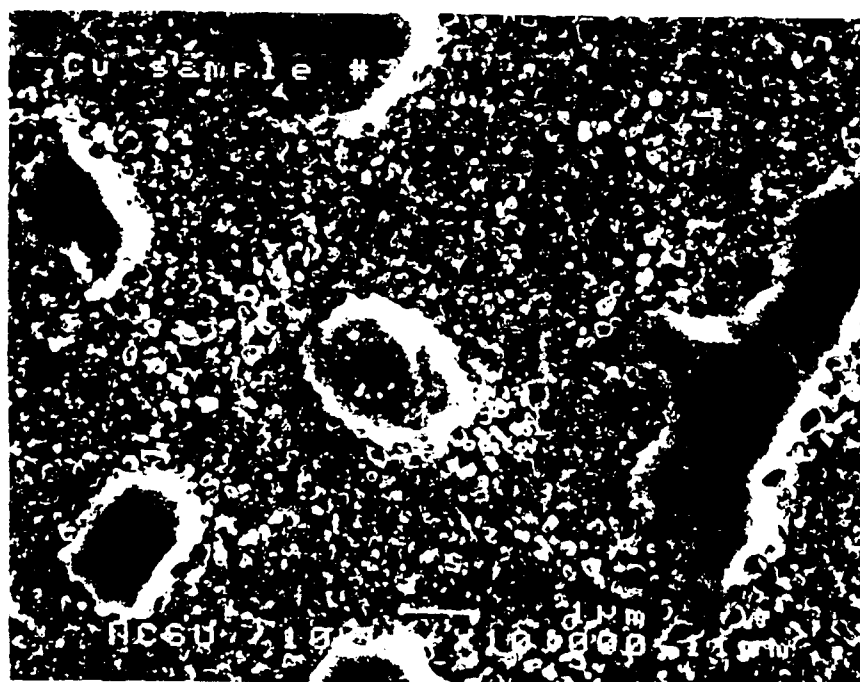


Figure 2 Cu samples implanted with a dose of 1×10^{18} ions/cm², an energy of 150 keV and a beam angle of 10° (sample 3). Note the network of amorphous or glassy globules, approximately 1 μm wide, resting on the surface which is covered by 100 nm size particles.

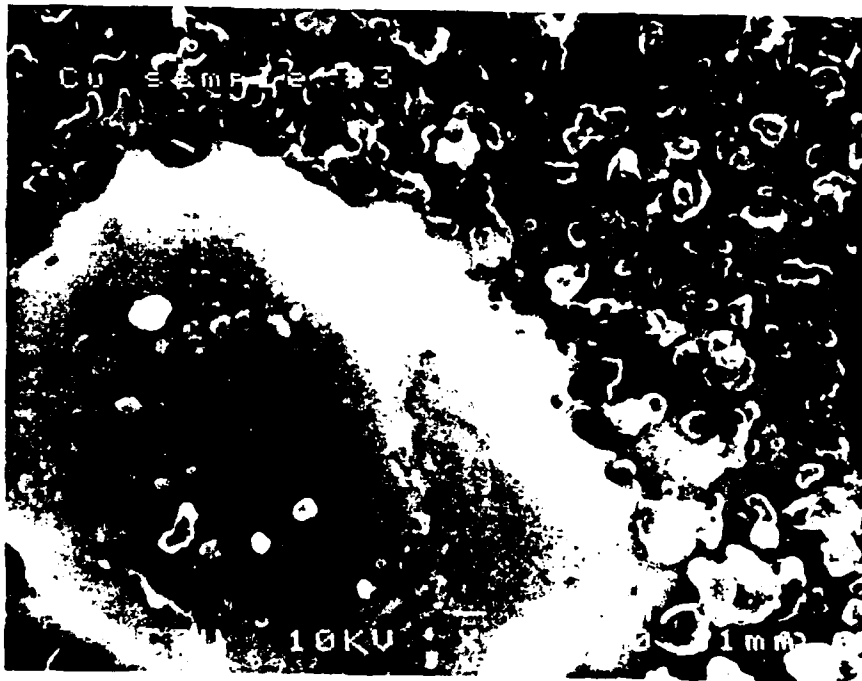


Figure 2(c). A magnified view of a large globule.

(a)



(b)



Figure 3 Cu samples implanted with a dose of 1×10^{18} ions/cm², an energy of 150keV and a beam angle of 10° (sample 4). This sample appears to have caves (a few μm in diameter) which are filled by irregularly shaped particles approximately 100nm in diameter.

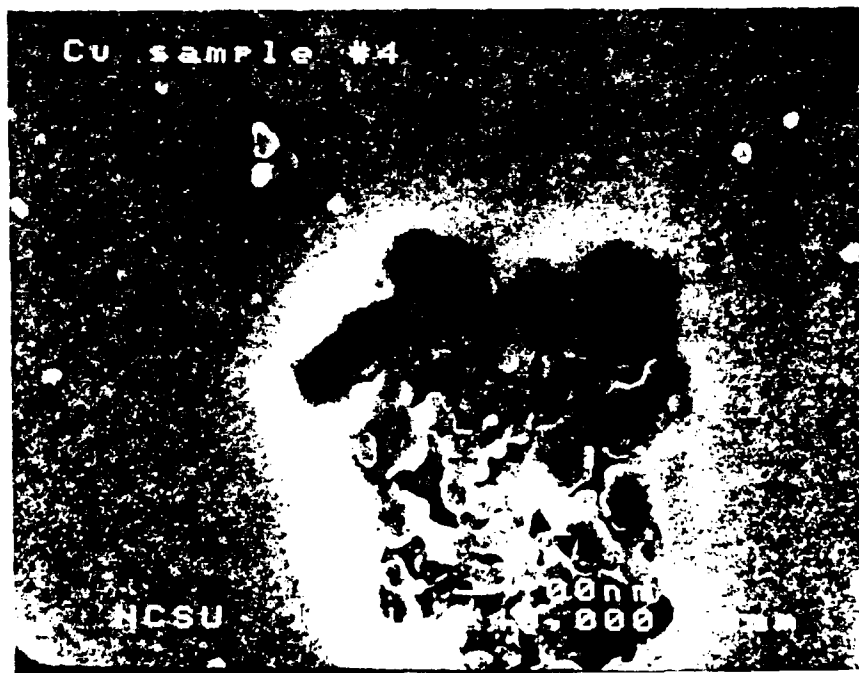


Figure 3(c). A magnified view of a cave indicates a smooth, glassy phase surrounding the cave - similar to the globules in Fig. 2.

Composition. The surface composition of the ion implanted copper was obtained via AES using a JEOL JAMP 30 Auger microprobe and via SIMS using a Cameca IMS 3f direct imaging microprobe. The samples were not pretreated in any way, and long exposure to the atmosphere had occurred prior to the analysis. The AES fine structure of the C KLL peak has been shown by Lurie and Wilson (Surf. Sci. 65, 476 (1977)) to be sensitive to the three allotropes of carbon. The shape of the fine structure of the low energy side of the carbon KLL peak can be used to distinguish between diamond, graphite and amorphous carbon as shown in Fig. 4. As illustrated the shape of the spectra obtained from the three allotropes are quite different. For diamond, the intensity of the fine structure peak closest to the primary C KLL peak is greater than the peak located at slightly lower energy. For graphite the fine structure peaks are reversed and for amorphous carbon there appears to be a mixture of the diamond and graphite spectra.

The Auger fine structure spectra for samples 1,2,3,&4 are shown in Fig. 5(a-e). All of the spectra contain the characteristic C KLL peak at 270eV accompanied by the peaks at lower energy which are used to determine the carbon allotrope(s) present on the surface. Fig. 5a represents the spectra from sample 1. It appears to have a close match to the graphite spectra shown in Fig. 4 and, therefore, the surface is composed of a graphite (sp^2) type of bonding. Fig. 5(b-e) represent the spectra for samples 3&4. All four spectra were obtained in the spot mode so that a more accurate assessment of the surface composition could be achieved. The SEM micrographs of these samples shown earlier had different surface morphologies, one sample containing globules on the surface and the other having a cave-like surface structure, thus, the spot mode was utilized to observe the difference, if any, in composition between these surface phenomena. Fig. 5(b,c) are spectra obtained from sample 3, Fig. 5b representing the spectra of a globule and Fig. 5c representing the spectra between the globules. Both spectra resemble the graphite spectra of Fig. 4. The cavelike sample is shown in Fig. 5(d,e) with Fig. 5d representing the spectra from inside the cave and

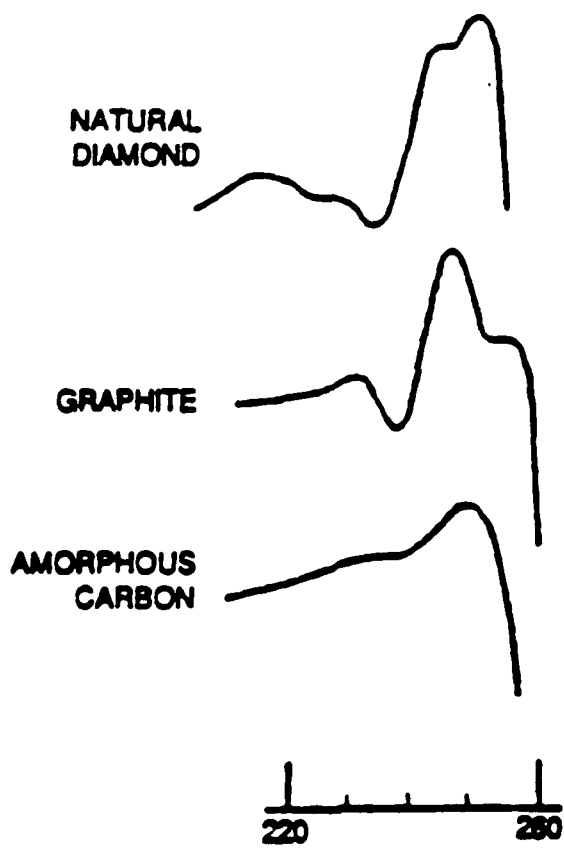


Figure 4. Auger fine structure spectra about the C KLL energy from Lurie and Wilson.

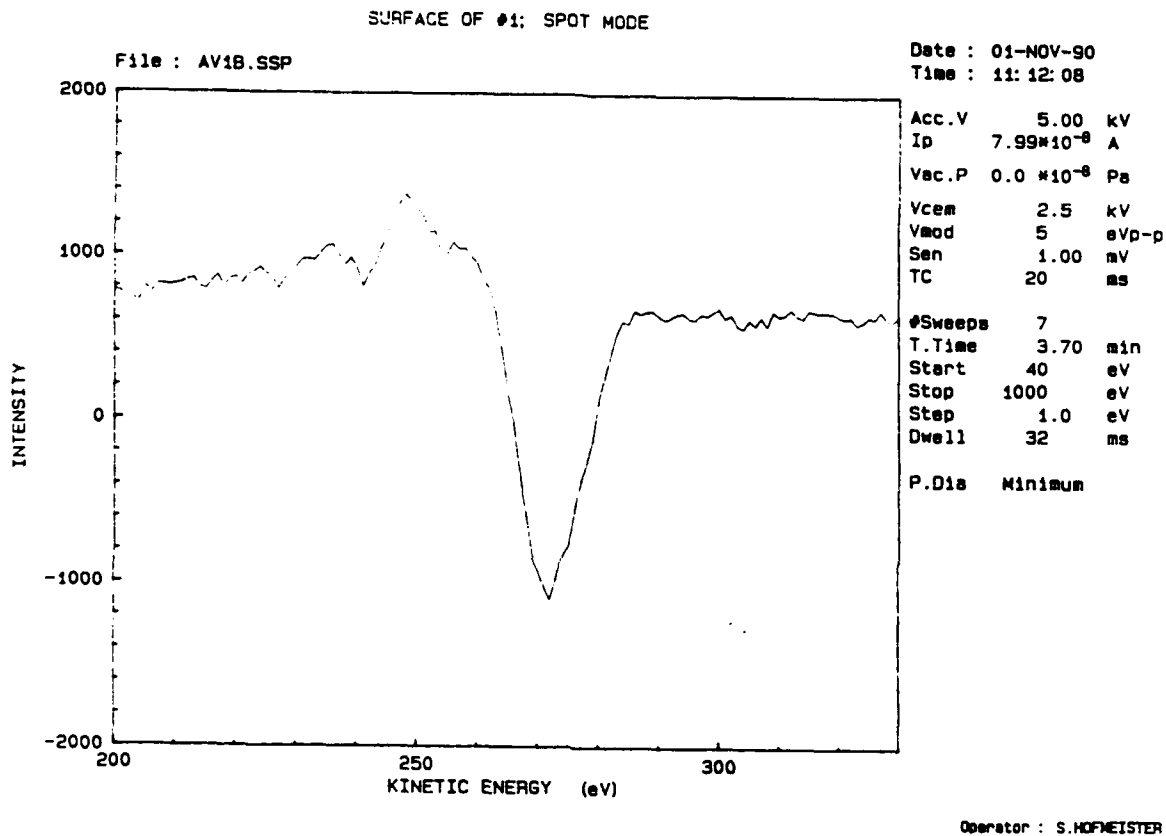
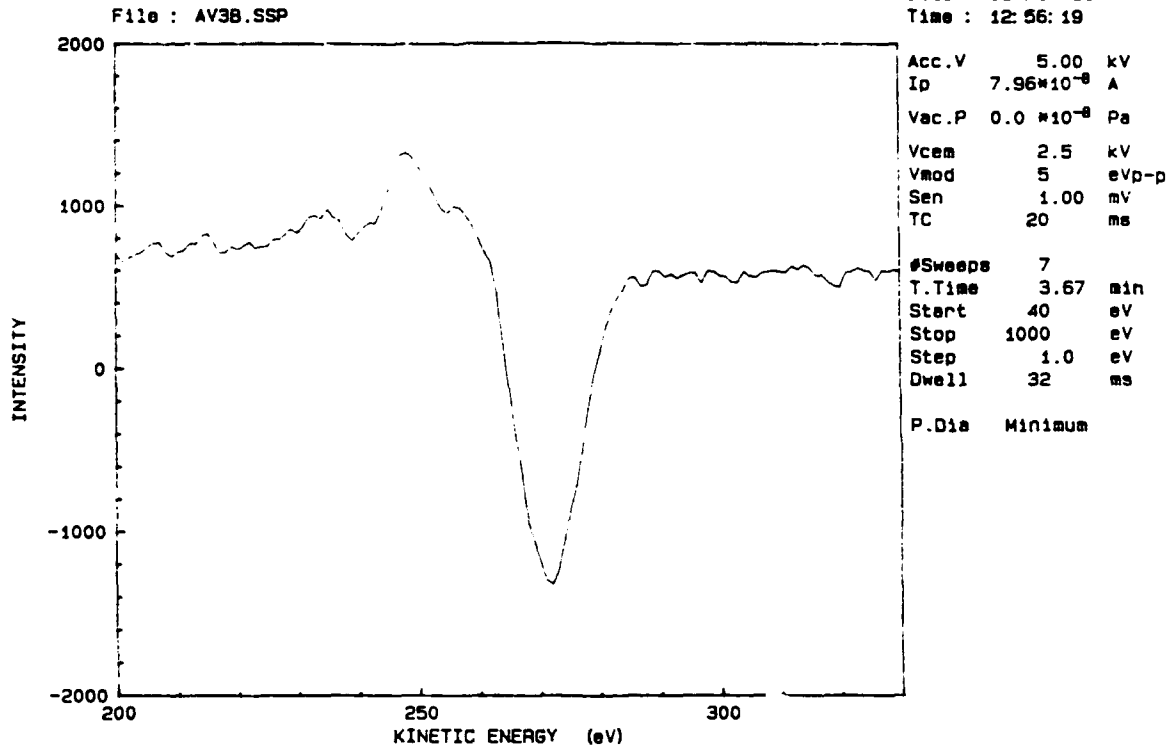


Figure 5. (a) Auger spectra from the Cu substrate implanted with a dose of 5×10^{17} ions/cm², an energy of 120keV and a beam angle of 0°. It appears to have a close match to the graphite spectra of Fig. 4. (b-e) Auger spectra from Cu samples implanted with a dose of 1×10^{18} ions/cm², an energy of 150keV and a beam angle of 10°.

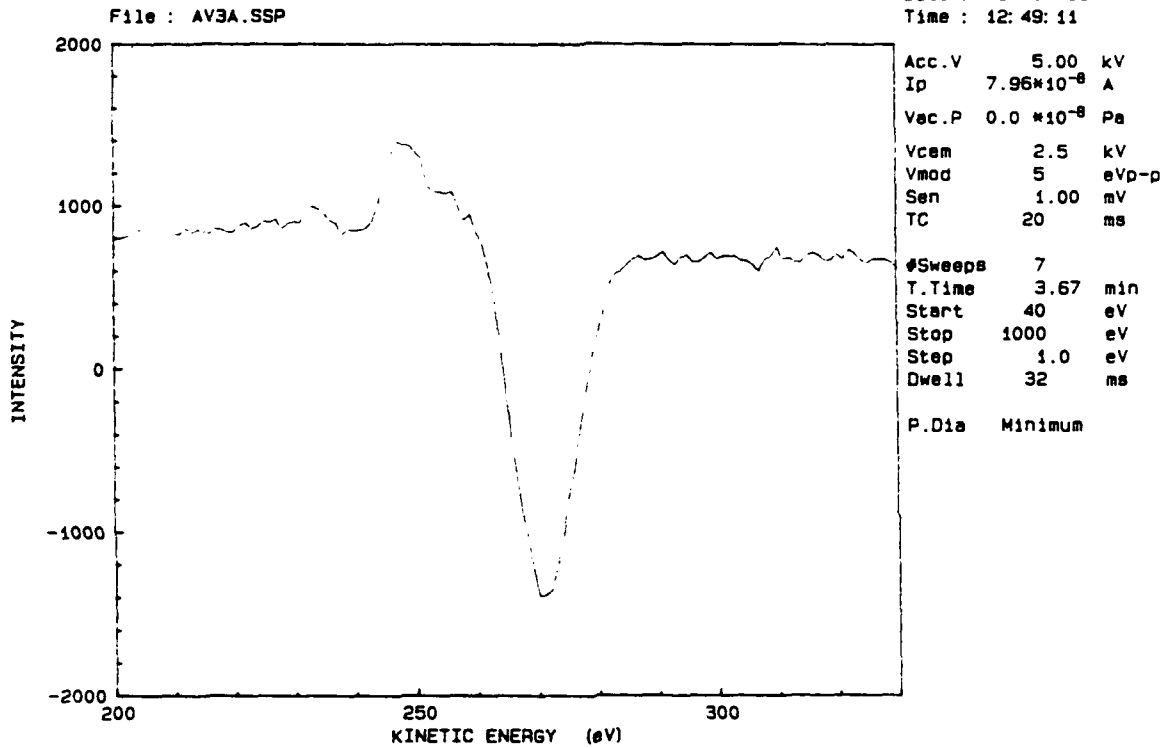
SURFACE OF #3; ON RIDGE



Operator : S.HOFMEISTER

Figure 5(b). Spectra from a globule.

SURFACE OF #3; BETWEEN RIDGES



Operator : S.HOFMEISTER

Figure 5(c). Spectra between the globule.

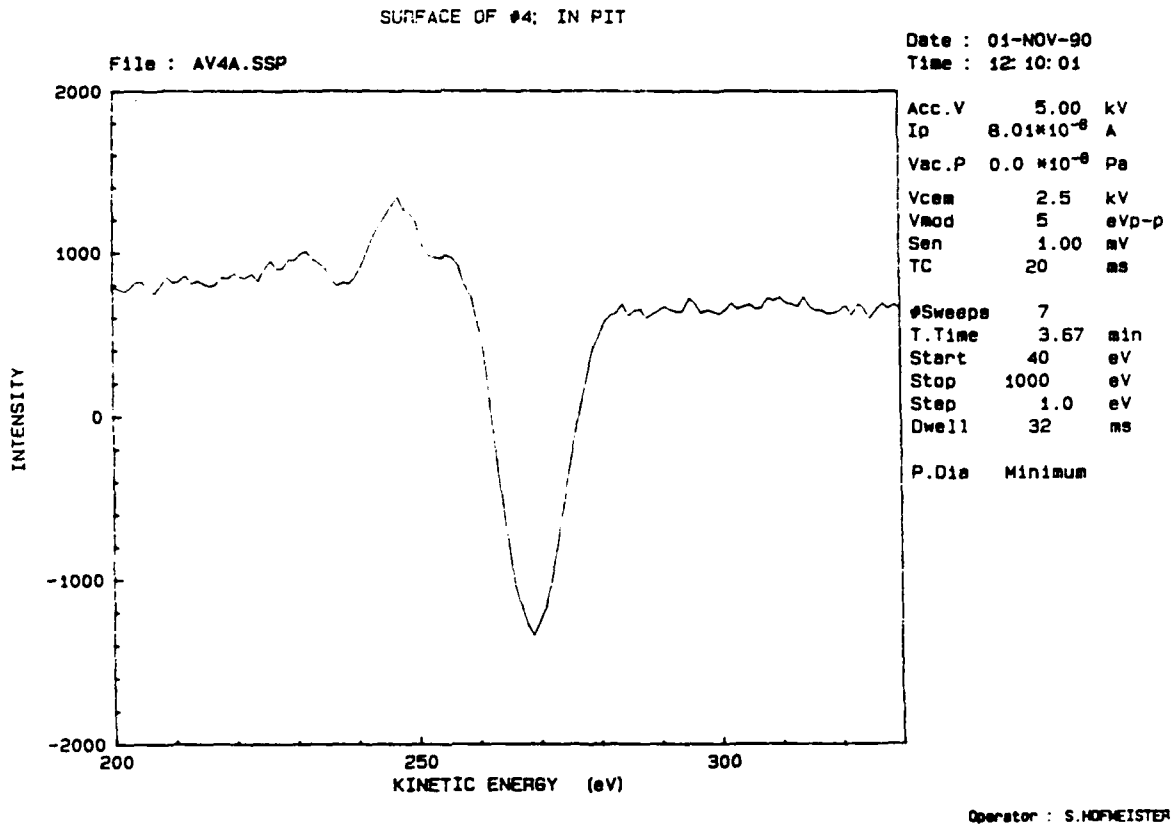


Figure 5(d). Spectra inside the cave.

SURFACE OF #4; OUTSIDE PIT

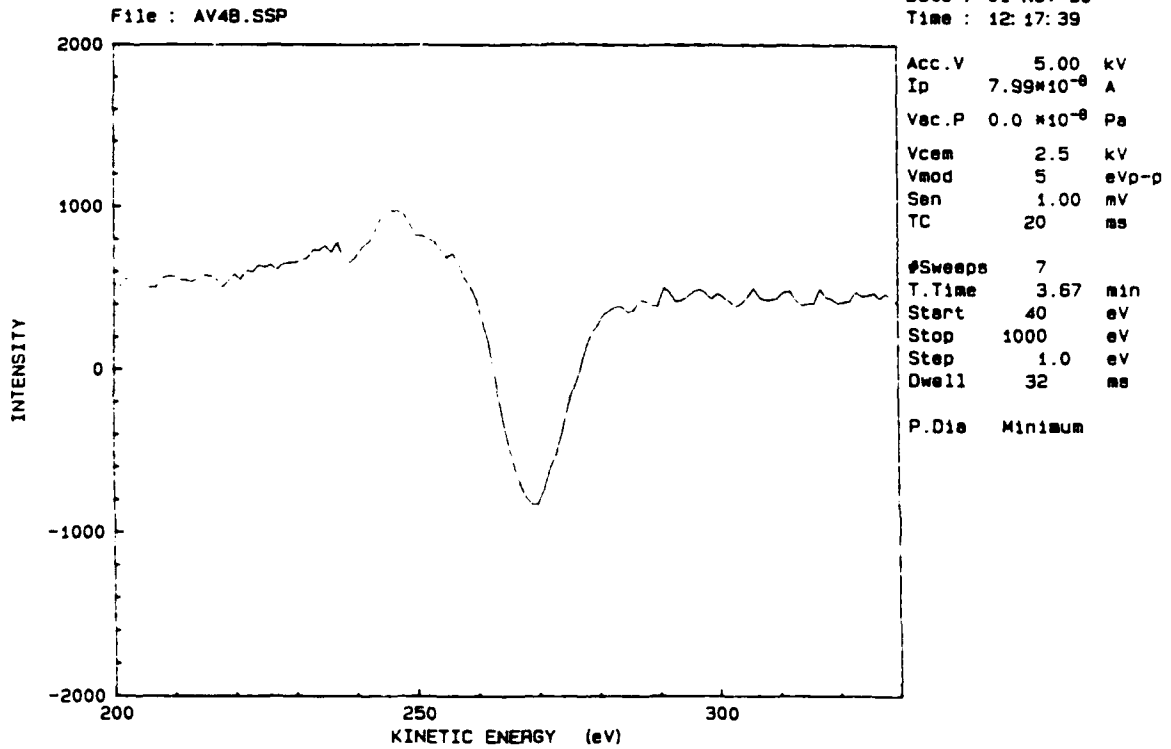


Figure 5(e). Spectra outside the cave.

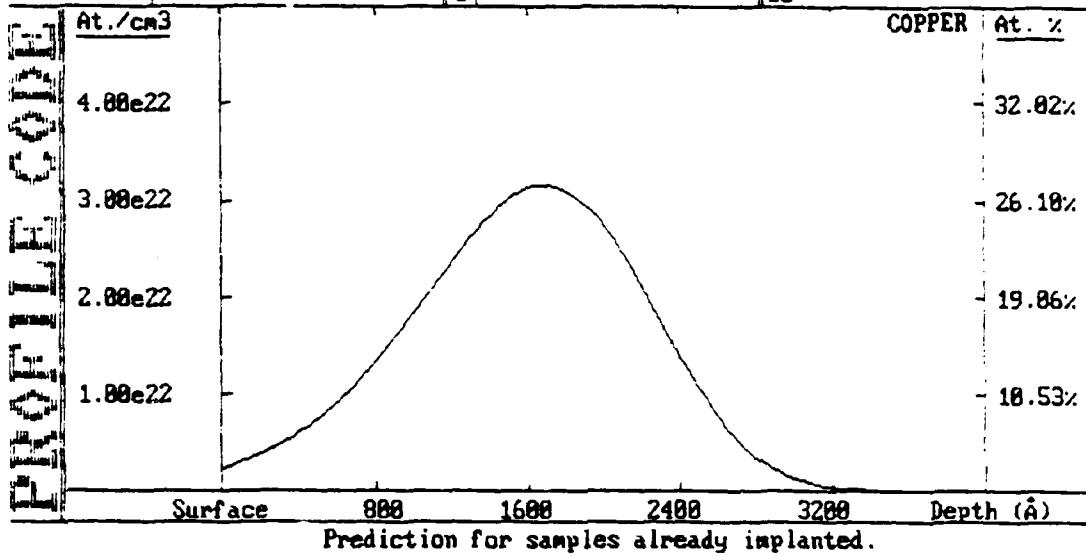
Fig. 5e representing the spectra outside the cave. Once again, both spectra resemble the graphite spectra of Fig. 4.

Another point mentioned earlier about these samples was that the cavelike morphology was caused by the globules growing until they connected leaving clusters of the smaller (10nm) particles uncovered. Comparison of the AES spectra for the globules of Fig. 2 and the glassy phase on the cavelike sample of Fig. 3 are almost identical, see Fig. 5b and Fig. 5d. The cavelike area and the region between the globules also have identical AES spectra, thus, verifying the idea about the different globule sizes, or an increased particle clustering in one sample as compared with the other, in the two samples.

SIMS was utilized to study the depth of the C implants in the Cu substrates. Using the Planar Pearson model, an estimate of the depth profile for the implants was realized, as illustrated in Fig. 6a, and Fig. 6b. This calculation did not consider the high temperature (900°C) used during the implant. It is interesting to note the high concentration of C at the projected range: approximately 30 at % C at 1600Å for the 120keV, 5.00 e17, 0° beam angle implant, and 40 at %C at a depth of 2000Å for the 150keV, 1.00e18, 10° beam angle implant. SIMS analysis was conducted utilizing a cesium primary beam to identify C and Cu by scanning a 50µm X 50µm area with the resulting spectra shown in Fig. 7(a-d). The low energy implants yielded C as deep as 0.75µm into the Cu sample with a relatively uniform distribution of C up to the C-Cu interface. The high energy, high dose implants yielded higher counts/s with a nonuniform C distribution and very different depth profiles. Fig. 7c represents the sample with the unattached globules and shows a gradual drop in C concentration with depth rather than the expected abrupt C-Cu interface. The lack of C moving to the free surface of the Cu could be the reason since the globules, identified as graphite using AES, in this sample are not connected to each other like the other sample. Also, the peak distribution is not uniform - there is an abrupt drop in count/s at approximately 25µm from the free surface. Fig. 7d has a different profile than Fig. 7c. It has a higher counts/s and the peak is smooth up to the interface at an approximate depth of 0.75µm. The concentration of C in Cu

TARGET=	COPPER	8.966	0°	keV	Ion Dose/cm2	keV	Ion Dose/cm2
Calc. Type	Planar, Pearson IV	1		120	C -12	5.00e17	6
Peak Data	1685Å 3.16e22 27.1%	2					7
Sput. Loss	Coef=.441 Tot.= 268Å	3					8
Retn. Dose	4.83e17/cm2 96.8%	4					9
		5					10

(a)



TARGET=	COPPER	8.966	10°	keV	Ion Dose/cm2	keV	Ion Dose/cm2
Calc. Type	Planar, Pearson IV	1		150	C -12	1.00e18	6
Peak Data	2020Å 5.49e22 39.3%	2					7
Sput. Loss	Coef=.373 Tot.= 433Å	3					8
Retn. Dose	9.63e17/cm2 97.9%	4					9
		5					10

(b)

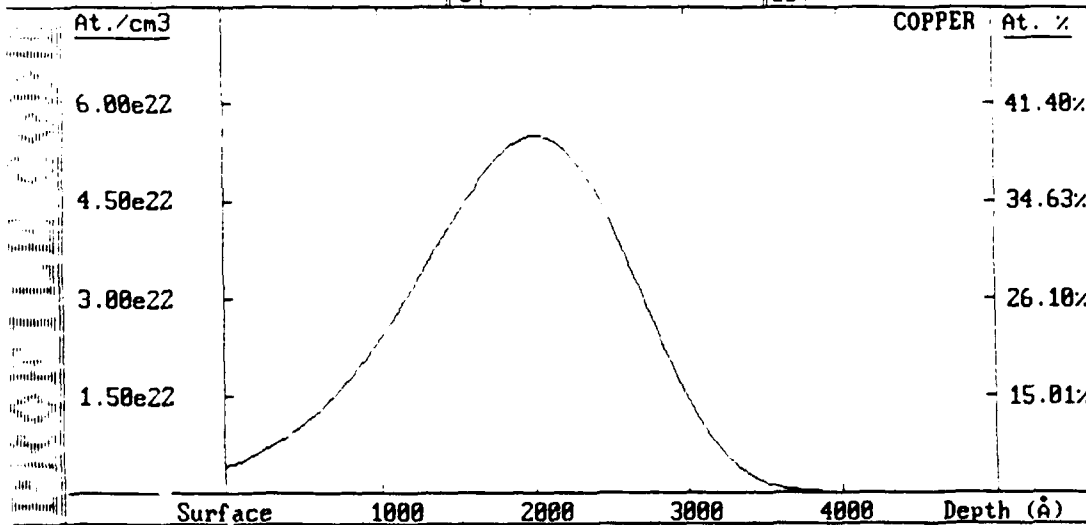


Figure 6. Planar Pearson profiles for: (a) a dose of 5×10^{17} ions/cm², an energy of 120keV and a beam angle of 0°, (b) a dose of 1×10^{18} ions/cm², an energy of 150keV and a beam angle of 10°. This calculation did not consider the high temperature used during the implantation.

can be calculated if it could be compared to a standard. Unfortunately, a standard was not available for the comparison

In all of the SIMS plots the Cu background follows the same path as the C profile up to the point of intersection where it flattens out. This could be due to the presence of oxygen near the surface, since Cu and oxygen tend to bond fairly easily and the incident ion beam would tend to break the Cu-O bond, thus, sputtering at a higher rate and therefore showing a higher concentration of Cu at the near surface region than expected. The oxygen could be present in the bulk due to the presence of an oxide layer on the surface prior to the implantation or perhaps the oxygen in the CO₂ gas source used in the implantation was not completely removed.

Conclusion. Carbon ion implantation into copper resulted in a graphitic surface phase. Scanning electron microscopy showed some very interesting surface phenomena on the high energy, high dose implants. AES showed the presence of graphite on the surface and proved to be helpful in determining the composition and explaining the difference in surface morphologies of the two samples implanted at high energy and high dose. SIMS gave an approximate depth profile of the C within the Cu substrate but the Cu profile was not normal. It remains a mystery as to how Prins was able to form a diamond film on the Cu surface under the same implantation conditions as we had attempted—perhaps we were not told everything.

E. The Use of Surfactants to Alter the Surface Energies of the Substrate and Diamond Film

The combination of surface free energies, interface free energy and lattice strain determine whether-or-not an epitaxial film will undergo 2-(layer-by-layer) or 3-(island) dimensional growth or a combination of initial layer-by-layer followed by island growth. The last phenomenon occurs in the case of pseudomorphic growths where the lattice parameters of the substrate and film are closely (not exactly) matched such that the film must be biaxially and elastically strained such that it comes into registry with the substrate. Continued deposition increases the total strain sufficiently such that 3-dimensional growth will occur.

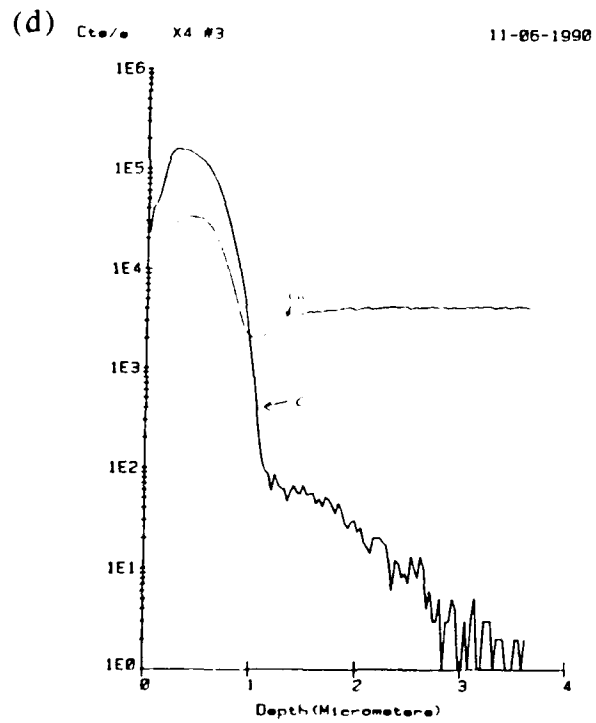
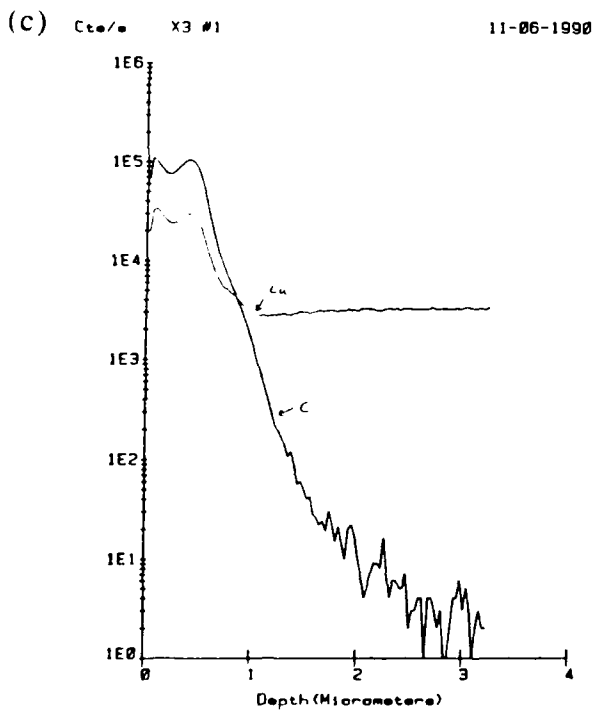
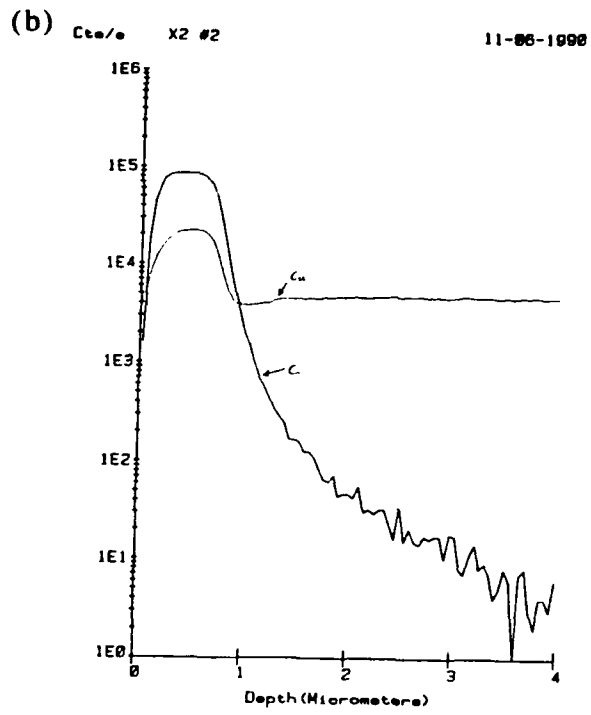
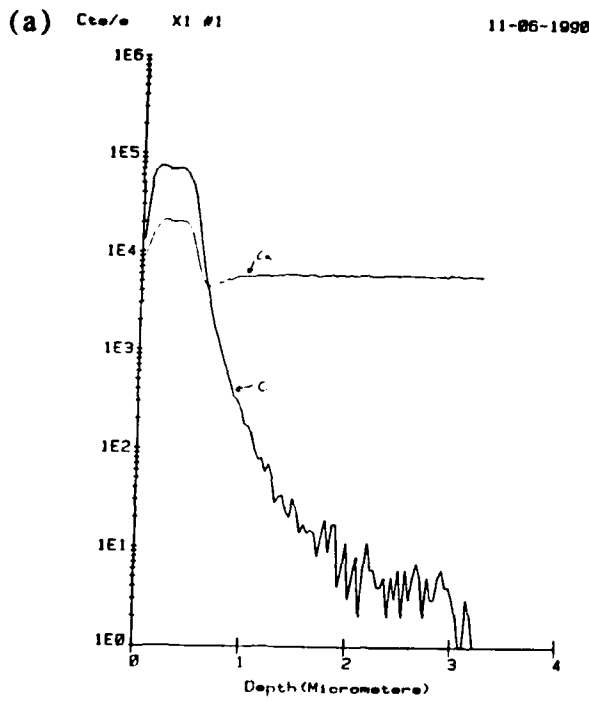


Figure 7. SIMS spectra for the C implanted Cu samples. (a & b) Profile for the Cu substrates implanted with a dose of 5×10^{17} ions/cm², an energy of 120keV and a beam angle of 0°. The approximate C depth is 0.75 μ m. (c & d) Profile for the Cu samples implanted with a dose of 1×10^{18} ions/cm², an energy of 150keV and a beam angle of 10°.

This latter phenomenon may also occur if there is interface mixing and/or surface reconstruction.

There is no known direct thermodynamic route to increase the surface energy of any substrate sufficiently such that this energy is greater than the sum of the surface energy of the diamond film + the diamond/substrate interfacial energy + the strain energy and, therefore, 2-dimensional nucleation and growth would occur. The surfactant route provides a thermodynamic route to solve a thermodynamic problem with a kinetic solution.

The thermodynamic problem is that a diamond nucleus without H on its surface will not wet the surface of any substrate of which we are aware. The thermodynamic route is the use of a surfactant which lowers the surface energy of both the substrate and the diamond film and which allows the diamond to retain the sp^3 bond at the surface of the growing film. The kinetic solution is that the C atoms which originally had sufficient mobility and time to form islands when C was deposited on a bare surface are now kinetically inhibited in terms of surface diffusion (since they are now covered by a capping layer) and in terms of chemical interdiffusion because the driving force of surface energy reduction via interdiffusion is now removed because they are no longer on the surface. However, if interfacial strain is created between the embedded layer and the substrate and, also, if the species of the embedded layer are soluble in the substrate under these conditions, interdiffusion should occur.

The substrate must be closely lattice matched (the lattice parameter of the film could be an integer multiple of that of the substrate). Thus, we are left with Ni, Cu, or cBN for the deposition of diamond, if we are to achieve 2-dimensional growth. Otherwise, the elastic strain will cause the nucleation and growth to be 3-dimensional. Even with the use of a surfactant, the strain is not relieved enough to prevent 3-dimensional growth.

The selection of a good surfactant for the Ni or Cu substrates is rather limited. Getting the C underneath the surfactant and then getting it to form sp^3 bonds in the diamond crystal lattice on the surface of the substrate is going to be a problem. Ni or Cu or cBN are crystallographically close to diamond but the bonding is the question. Most any gaseous

species should lower the surface energy of Cu or Ni and diamond and any monolayer of F or Cl would be a good choice at the moment. Since, a C containing gas species would not be able to get through the adsorbed gas without the common reactions that are currently being employed to achieve diamond, the best way may be to get the C to come to the surface from within the Cu or Ni. This has always created graphite during deposition or straight segregation.

Perhaps, as was mentioned by Max Yoder, of ONR, if the metal was saturated with H and C at high temperature, annealed at lower temperature in a continuous flow of F or Cl or even H and see if the C will diffuse to and across the surface while connected to a gaseous species and tie up with other C species to give an sp^3 bond. Cu should be the best substrate in this case since the solubility of C is very low at all temperatures. The C would be introduced via implantation and the host crystal heated in a gradient so that the C will come to the desired surface. This method will be looked into with more detail in the near future.

F. Summary and Future Plans

As stated, the goal of this study is to achieve epitaxial growth of single crystal diamond films on one or more nondiamond substrates. The research vectors outlined above are: (a) high pressure, (b) ion beam enhanced epitaxy, (c) carbon ion implantation into Cu, and (d) the use of surfactants. The high pressure work will be done at Los Alamos National Laboratory under the guidance of Dr. Dave Schefferal and also Dr. Michael Paesler at NCSU. Sample preparation for the diamond anvil cell is already underway and a trip to Los Alamos will be planned for January, 1991. Samples, with rf sputtered amorphous C films, have been sent to Dr. Bruce Sartwell for H-content determination and to Dr. James E. Butler for Raman analysis, who are both at the Naval Research Laboratory in Washington D.C.

The ion beam enhanced epitaxy project will be conducted at Oak Ridge National Laboratories under the supervision of Dr. Stephen Withrow. This project will be underway as soon as Dr. Withrow is able to get beam time. The ion implantation of C into Cu was not

successful in forming a diamond film and needs to be pursued further. The surfactant project is still in the planning stages but once we find a suitable surfactant it will be underway.

IV. Electronic Devices Fabricated From Diamond

A. Introduction

Electronic devices such as MESFETs fabricated from semiconducting diamond may offer improved RF performance relative to comparable devices fabricated from commonly used semiconductors such as Si and GaAs. In particular, the material properties of diamond indicate the potential for devices with high RF output power and high frequency capability.

Although the optimum RF performance should be attainable from n-channel devices due to superior electron transport characteristics compared to that of mobile holes, the difficulty in producing suitable n-type semiconducting crystals has resulted in interest in fabricating devices from p-type material. Natural diamond is often p-type due to boron impurities, and synthetic diamond can be doped with boron with relative ease. It is likely, therefore, that the first high performance MESFETs fabricated in diamond will have p-type conducting channels. Most of the device results presented to date have been on p-type diamond and most current work in progress is directed towards the development of p channel devices on both natural and synthetic p-type material due to the relative ease of obtaining suitable crystals.

The use of p-type material presents an interesting problem. Most investigations of boron impurities in diamond (e.g., doping by ion-implantation) indicate an activation energy of about 0.37 eV. This, in turn, indicates that the device must be operated at high temperatures (about 500 °C) in order to activate the impurities. Operation at elevated temperature, however, results in rapid degradation of the hole mobility, which decreases with temperature according to a $T^{-2.8}$ law. This, in turn, will reduce the channel current that can flow in the device, thereby significantly reducing the RF output power attainable.

It should be noted that there is some discrepancy in the activation energies reported for boron in diamond. For example, Wentorf (1962) has reported an activation energy of 0.17-0.18 eV for boron doping in synthetic diamond crystals formed at high

temperature and high pressure out of mixtures of graphite and Fe-Ni catalyst metal. Fujimori (1986) has reported an activation energy of 0.013 eV for boron doped into the diamond during crystal growth by vapor phase deposition. The value of activation energy is important relative to the question of device operating temperature. Room temperature operation is, of course, desirable in order to obtain good RF output power, gain and conversion efficiency without the need to use energy consuming devices such as heaters. Room temperature operation requires a relatively low value for the activation energy. The lower value of activation energy (0.013) would permit room temperature operation; whereas, an activation energy of 0.37 eV will require the high temperature conditions.

This report presents an investigation of the microwave performance potential of p-type diamond microwave MESFETs. A device was designed for optimum operation at X-band (10 GHz) and its RF performance was simulated at both room temperature and 500 °C. The simulations should provide a realistic assessment of the potential of this type of device for microwave RF power applications.

B. Simulation Results

The device model employed in this work is a physics based simulation that includes all relevant physical phenomena known to be of significance to the practical operation of the device. Of particular interest in this work is the temperature dependence of charge carrier transport and breakdown voltage. Charge mobility is modeled according to an inverse temperature law ($\mu_h \sim T^{-2.8}$ for holes in semiconducting diamond). The temperature rise over ambient is determined with knowledge of the device thermal resistance, which is calculated from a theoretical model. The thermal resistance model used in this work has been verified with experimental data taken on GaAs MESFETs. The thermal resistance is multiplied by the power dissipated in the device channel to obtain the channel temperature rise.

The MESFET design was designed to produce optimum power-added efficiency at 10 GHz. The device has a gate length of $L_g=0.5 \mu\text{m}$, a gate width of $W=1 \text{ mm}$ with ten gate fingers. The channel has uniform doping with a boron concentration of $N_a=4 \times 10^{17} \text{ cm}^{-3}$ with a channel depth of $a=0.15 \mu\text{m}$. The source-gate and source-drain spacings are both $1 \mu\text{m}$. The contact resistance was assumed to have a value of $R_c=10^{-4} \text{ W-cm}^2$, which is in agreement with the best values reported thus far. The gate metal is gold. The critical material and device parameters used for room temperature and 500°C operation are listed in Table I.

Table I. Material and Device Parameters used in MESFET Model at Room Temperature and 500°C

Parameter	Room Temp.	500°C
Thermal Conductivity	$30 \text{ W/}^\circ\text{K-cm}$	$14 \text{ W/}^\circ\text{K-cm}$
Device Therm. Resistance	$0.73 \text{ }^\circ\text{K/W}$	$1.57 \text{ }^\circ\text{K/W}$
Hole Mobility	$600 \text{ cm}^2/\text{V-sec}$	$100 \text{ cm}^2/\text{V-sec}$
Hole saturated velocity	$1.08 \times 10^7 \text{ cm/sec}$	$1.08 \times 10^7 \text{ cm/sec}$
Breakdown voltage	92.4 v	70 v

The dc I-V characteristics for the device at room temperature and 500°C are shown in Figs. 1 and 2, respectively. The calculations were performed assuming 100% activation. The validity of this assumption is, of course, directly dependent upon the value for the activation energy of the boron impurities. Operation at the elevated temperature significantly affects the device performance. The maximum channel current (i.e., I_{dss}) is reduced from about 400 mA to about 245 mA, almost a 40% reduction, and the maximum dc transconductance is reduced from about 50 mS/mm to

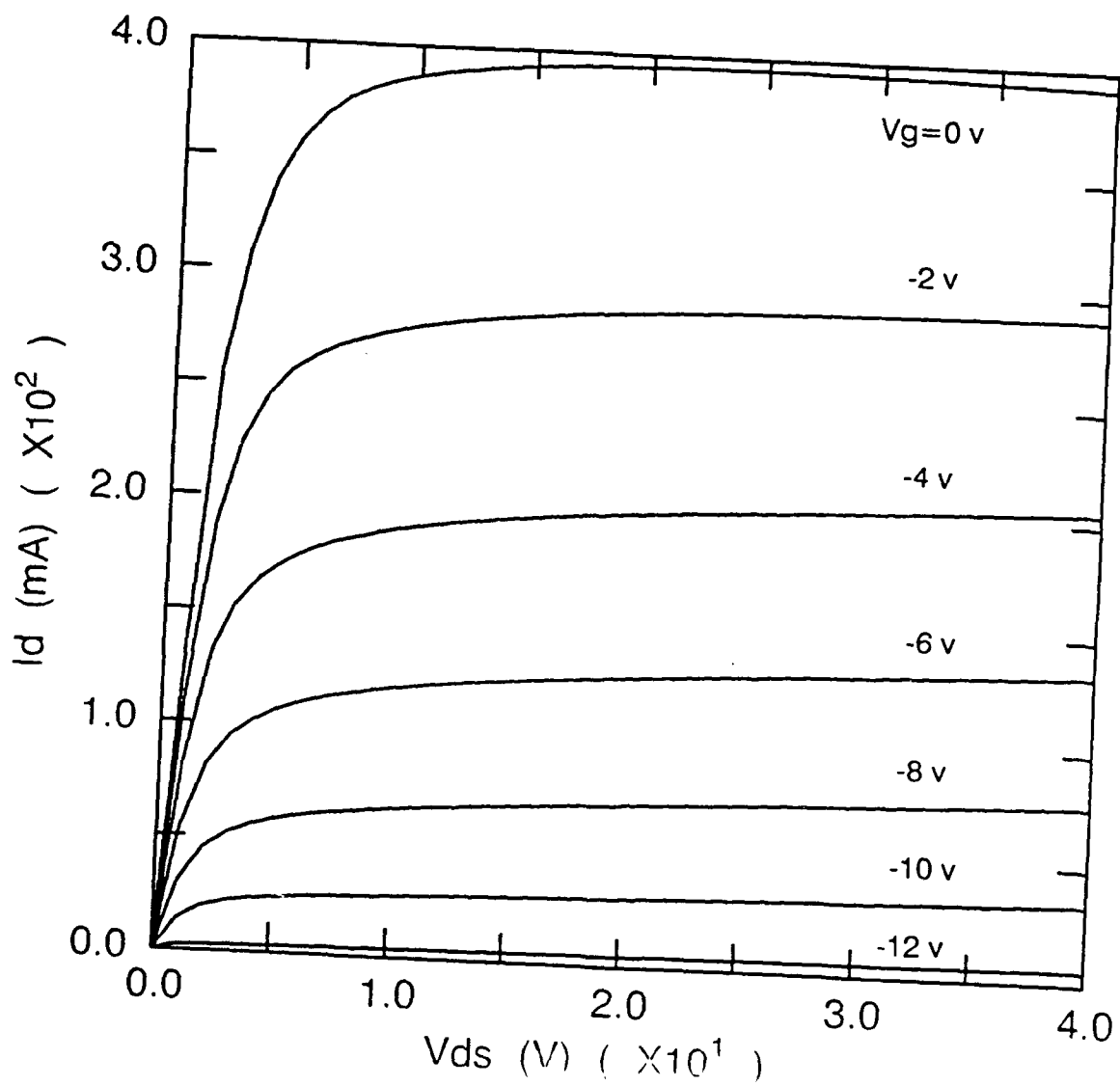


Figure 1. dc I-V Characteristics for a p-type Diamond MESFET ($L_g=0.5 \mu\text{m}$, $W=1\text{mm}$, Room Temperature Operation)

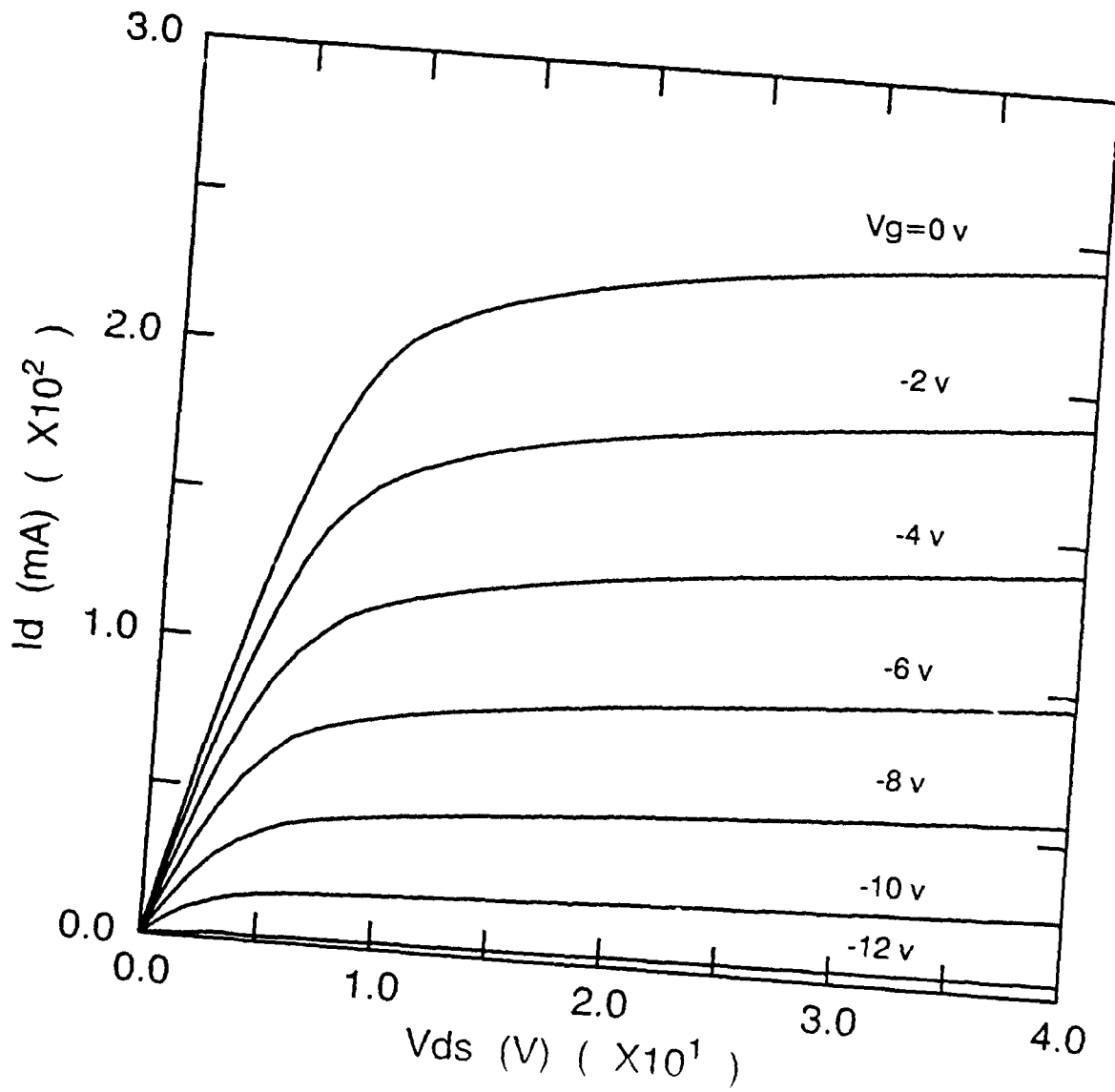


Figure 2. dc I-V Characteristics for a p-type Diamond MESFET ($L_g=0.5 \mu\text{m}$, $W=1\text{mm}$, 500°C Operation)

25 mS/mm. Also, the drain voltage required to achieve saturation conditions is increased from 5 v to about 10 v.

In the RF simulations the device was biased for class A operation with a bias voltage of $V_{ds}=40$ v and $I_{ds}=I_{dss}/2$. The device was operated in a microwave circuit and the circuit was tuned to produce maximum power-added efficiency (PAE) at a frequency of 10 GHz. The RF output power, gain, and power-added efficiency are shown in Figs. 3, 4, and 5, respectively. At room temperature the device produces 37.7 dbm (5.9 W/mm), 12.2 db gain, and 50.6% PAE. At 500 °C the RF performance is degraded, but the device still produces 32.9 dbm (1.9 W/mm), 9.9 db gain, and 37% PAE.

C. Discussion

The results of the simulations indicate that p-type diamond MESFETs can be used to generate microwave power with good results, even if high temperature operation is necessary. The simulations indicate that room temperature and 500 °C operation of these devices produce RF output power approximately 6 times and 2 times that available from GaAs MESFETs operating under room temperature ambient conditions. GaAs MESFETs are currently limited in RF output power capability to about 1 W/mm of gate width.

A problem not addressed in this work concerns the effects of excessive gate leakage current. Currently, most reported attempts to fabricate diamond MESFETs have encountered excessive gate leakage, the cause of which is not currently understood. The excessive leakage severely limits the RF output power that can be obtained since the gate leakage current prevents high drain bias voltages from being applied. The low hole mobility requires that high drain bias and short gate lengths be employed in order to achieve current saturation conditions in the conducting channel. Most reported attempts to limit the leakage current have been directed towards the use of oxide or highly resistive layers directly under the metal gate. Although these

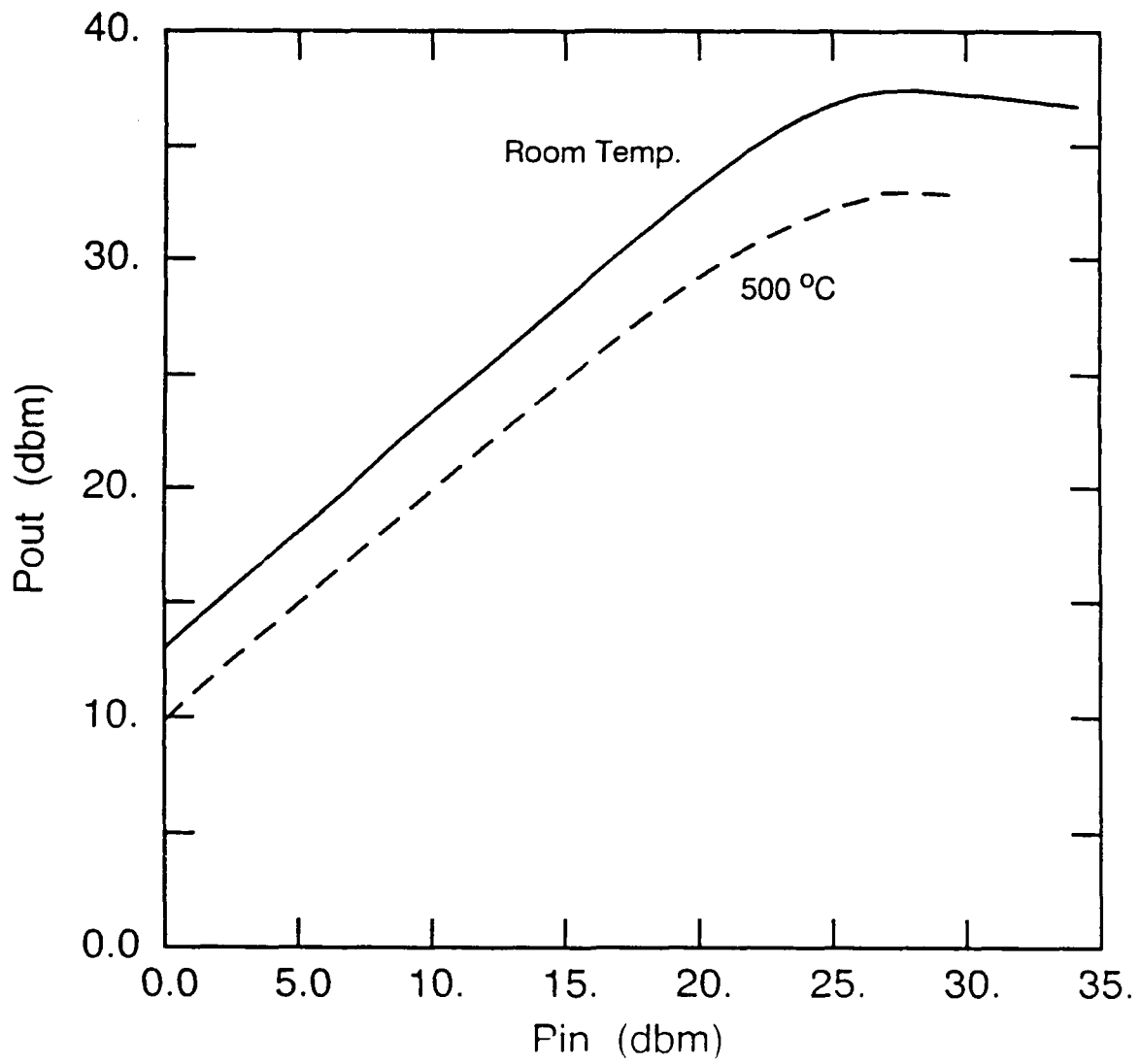


Figure 3. RF Output Power vs. Input Power at 10 GHz for a p-type Diamond MESFET ($L_g=0.5 \mu\text{m}$, $W=1 \text{ mm}$, Class A Operation, $V_{ds}=40 \text{ v}$)

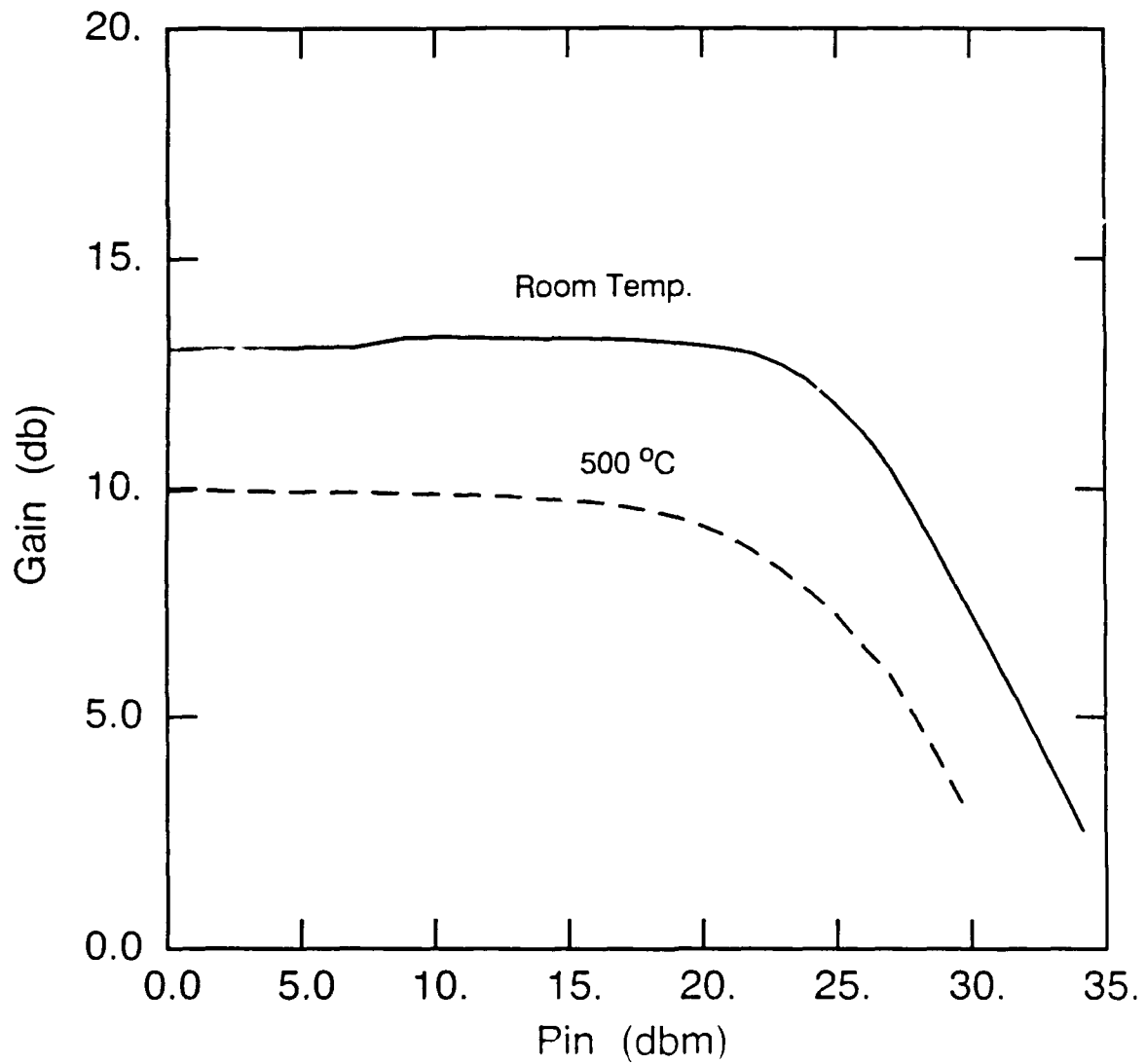


Figure 4. Gain vs. Input Power at 10 GHz for a p-type Diamond MESFET ($L_g=0.5 \mu\text{m}$, $W=1 \text{ mm}$, Class A Operation, $V_{ds}=40 \text{ v}$)

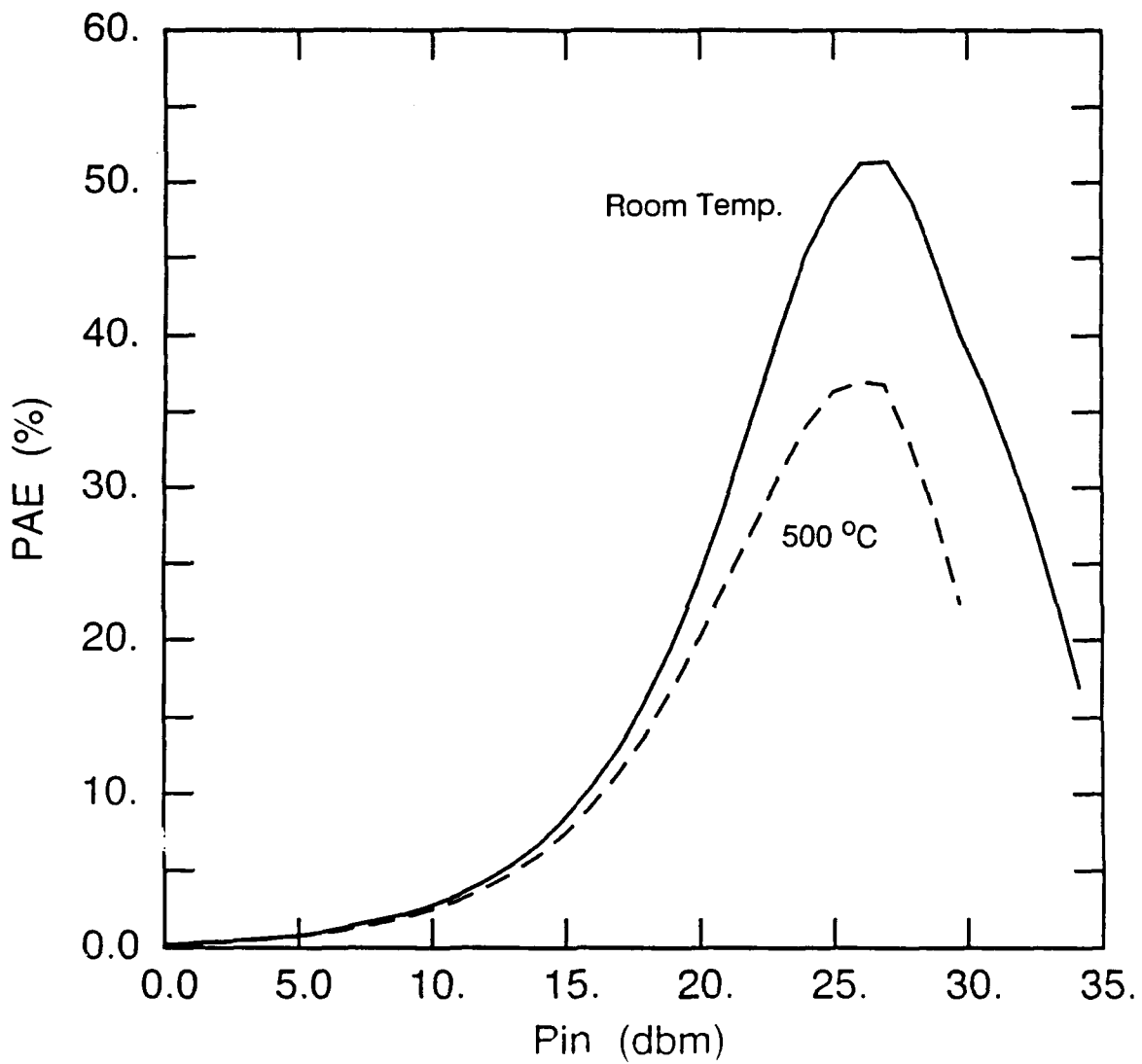


Figure 5. Power-Added Efficiency vs. Input Power at 10 GHz for a p-type Diamond MESFET ($L_g=0.5 \mu\text{m}$, $W=1 \text{ mm}$, Class A Operation, $V_{ds}=40 \text{ v}$)

techniques reduce gate leakage current, they also degrade the RF performance of the device due to reduced gain.

We are currently developing a theory of gate leakage for MESFETs. The theory developed to date is in excellent agreement with experimental observations on GaAs MESFETs and, in fact, is the only theory presented so far that can explain the detailed behavior of gate-drain breakdown in these devices. The theory postulates that the leakage is due to a tunneling of charge carriers from the metal gate to the surface of the semiconductor between the gate and drain electrodes. The surface charge flows between the two electrodes, thereby creating the excessive leakage current. Since the tunneling mechanism is enhanced at elevated temperature, the gate leakage increases as operating temperature is increased. This mechanism is responsible for the observed decrease in gate-drain breakdown voltage as temperature increases.

We believe that a similar tunneling and surface conduction mechanism is responsible for the excessive gate leakage observed in diamond MESFETs. The successful development of these devices will require that suitable techniques for reducing the surface currents be determined. This can most likely be accomplished by means of suitable surface treatments.

D. Conclusions

The microwave operation of p-type diamond MESFETs at room temperature and 500 °C ambient conditions has been theoretically investigated. Simulations performed at 10 GHz for a MESFET operating under class A tuned circuit conditions indicate that the device can produce approximately 6 and 2 W/mm RF output power with power-added conversion efficiencies of about 50% and 37% for the two temperatures, respectively. This indicates that the relatively low hole mobility of boron doped diamond does not prevent high performance microwave devices from

being fabricated. The RF performance compares quite favorably with the approximately 1 W/mm possible from comparable GaAs devices.

Realization of the indicated results will require that suitable techniques for reducing the excessive gate leakage current be developed. The excessive leakage current limits the drain bias that can be applied, thereby preventing current saturation conditions from being achieved in the conducting channel. The gate leakage current can be reduced by development of suitable surface treatments.

E. Future Research

Future research will include further simulations on the high temperature operation of p-type diamond MESFETs. In particular, a theory for the excessive gate leakage current will be further developed. Techniques for reduction of the leakage current will be investigated.

V. Appendix
Distribution List—Annual Letter Report
Contract Number N00014-86-K-0666

Address	Number of Copies	Address	Number of Copies
Mr. Max Yoder Office of Naval Research Electronics Program—Code 1114 800 North Quincy Street Arlington, VA 22217	8	Dr. James Butler Naval Research Laboratory Code 6174 Washington, DC 20375	1
Office of Naval Research Resident Representative Georgia Institute of Technology 206 O'Keefe Building Atlanta, GA 30332-0490	1	James Mayer Materials Science and Engineering 210 Bard Hall Cornell University Ithaca, NY 14853	1
Director Naval Research Laboratory Attention: Code 2627 Washington, DC 20314	6	Dr. Bradford Pate Department of Physics Washington State University Pullmany, WA 99164-2184	1
Defense Technical Information Center Building 5 Cameron Station Alexandria, VA 22314	12	Professor Pankove Electrical and Computer Engineering University of Colorado Boulder, CO 80309-0455	1
Robert J. Markunas Research Triangle Institute Post Office Box 12194 Research Triangle Park, NC 27709-2194	1	Office of Naval Research Attention: Code 1131M Arlington, VA 22217	1
Michael W. Geis Lincoln Laboratories 244 Wood Street P. O. Box 73 Lexington, MA 02173	1	Naval Research Laboratory Attention: Code 4683 Washington, DC 20375	1
Professor N. Parikh Department of Physics University of North Carolina at Chapel Hill Chapel Hill, NC 27514	1	Naval Research Laboratory Attention: Code 6820 Washington, DC 20375	1
Professor Russell Messier 265 Materials Research Laboratory Pennsylvania State University University Park, PA 16802	1	Naval Research Laboratory Attention: Code 6211 Washington, DC 20375	1
		Naval Research Laboratory Attention: Code 6684 Washington, DC 20375	1

Naval Research Laboratory Attention: Code 4684 Washington, DC 20375	1	Professor G. Walrafen Chemistry Department Howard University 5325 Potomac Avenue, NW Washington, DC 20016	1
Dr. Jim Zeidler Naval Ocean Systems Center Attention: Code 7601 San Diego, CA 92152	1	Professor I. Lindau Synchrotron Radiation Laboratory Stanford, CA 94305	1
Naval Ocean Systems Center Attention: Code 911 San Diego, CA 92152	1	A. J. Purde Texas Instruments MS 147 P. O. Box 655936 Dallas, TX 75265	1
Naval Ocean Systems Center Attention: Code 56 San Diego, CA 92152	1	W. D. Partlow Westinghouse Research and Development Center 1310 Beulah Road Pittsburgh, PA 15235	1
Dwight Duston OSD/SDIO/IST Pentagon Washington, DC 20301-7100	1	R. L. Adams 21002 North 19th Avenue Suite 5 Phoenix, AZ 85027	1
DARPA/D.S.O. 1400 Wilson Boulevard Arlington, VA 22209	1	Professor John C. Angus Chemical Engineering Case Western Reserve University Cleveland, OH 44106	1
Professor R. F. Davis Materials Science and Engineering Box 7907 North Carolina State University Raleigh, NC 27695-7907	1	Prof. Thomas R. Anthony General Electric Corporation Research and Development Center Building K-1, Room 1CSO P. O. Box 8 Schnectady, NY 12301	1
Professor K. J. Bachmann Materials Science and Engineering Box 7907 North Carolina State University Raleigh, NC 27695-7907	1	Yehuda Arie SRI Sarnoff Center Princeton, NJ 08540	1
Professor R. J. Nemanich Department of Physics Box 8202 North Carolina State University Raleigh, NC 27695-8202	1	P. J. Boudreaux Laboratory for Physical Science 4928 College Avenue College Park, MD 20740	1
Professor R. J. Trew Electrical and Computer Engineering Box 7911 North Carolina State University Raleigh, NC 27695-7911	1	Professor R. F. Bunshaw University of California 6532 Buelter Hall Los Angeles, CA 90024	1
Dr. Sandor Holly Rocketdyne Division Rockwell International, MS FA03 Canoga Park, CA 91304	1		

Ray Calloway Aerospace Corporation Post Office Box 92957 Los Angeles, CA 90009	1	Paul Caldwell DASIAS Field Office 2560 Huntington Avenue Suite 500 Alexandria, VA 22303	1
Jerome J. Cuomo T. J. Watson Center Yorktown Heights, NY 10598	1	Defense Nuclear Agency ATTN: RAEE (CAPT Fore) Washington, DC 20305-1000	1
Professor P. H. Fang Department of Physics Boston College Chestnut Hill, MA 02167	1	Dr. Ian Brown Lawrence Berkeley Laboratory Bldg. 53 University of California Berkeley, CA 94720	1
Wen Hsu Sandia National Laboratories Division 8347 Box 969 Livermore, CA 94550	1	Dr. Andrez Badzian 271 Materials Research Laboratory The Pennsylvania State University University Park, PA 16802	1
Professor W. Lanford Physics Department S.U.N.Y. Albany, NY 12222	1	Prof. Jerzy Bernholc Department of Physics Box 8202 North Carolina State University Raleigh, NC 27695-8202	1
Professor E. S. Machlin 44 Morningstar Drive Croton-on-Hudson, NY 10520	1	Tarasankar DebRoy Materials Science and Engineering Penn State University 212 Steidle Building University Park, PA 16802	1
Michael Pinneo Crystallume 3180 Porter Drive, Suite 2 Palo Alto, CA 94304	1	Joe Beeler Materials Science and Engineering Box 7907 North Carolina State University Raleigh, NC 27695-7907	1
Kenneth Russell J. P. L. M. S. 122-123 4800 Oak Grove Drive Pasadena, CA 91109	1	Michael Frenklach Penn State University 202 Academic Projects Building University Park, PA 16802	1
Professor T. D. Moustakas Exxon Research Ammandale, NJ 08801	1	Maurice Landstrass Crystallume 125 Constitution Drive Menlo Park, CA 94025	1
Professor J. L. Davidson 200 Brown Hall Auburn University Auburn, AL 36849	1	Keppi Wu OSD/SDIO/IST Washington, DC 20301-7100	1
B. Meyerson IBM T. J. Watson Center Yorktown Heights, NY 10598	1		

Warren Pickett Code 4692 Naval Research Laboratory Washington, DC 20375-5000	1	Thomas Perry Physics Department GM Tech Center Warren, MI 48090	1
Ron Rudder Research Triangle Institute P. O. Box 12194 Research Triangle Park, NC 27709-2194	1	R. Hauge Chemistry Department Rice University P. O. Box 1892 Houston, TX 77251	1
John B. Posthill Research Triangle Institute P. O. Box 12194 Research Triangle Park, NC 27709-2194	1	Ken Stalder SRI International 333 Ravenswood Avenue Menlo Park, CA 94025	1
Howard Schmidt Schmidt Instruments 2476 Bolsover, Suite 234 Houston, TX 77005	1	C. Richard Guarnieri IBM Research Center Yorktown Heights, NY 10598	1
Dr. Skotheim Moltech Corporation Box 572 Woodville Road Shoreham, NJ 11786	1	William Banholzer K1-CEB G20, P. O. Box 8 Schenectady, NY 12301	1
Karl Spear Pennsylvania State University 201 Steidle University Park, PA 16802	1	Albert Feldman NIST Gaithersburg, MD 20899	1
Max Swanson Department of Physics University of North Carolina Chapel Hill, NC 27514	1	Dario Narducci IBM Research Division P. O. Box 219 Yorktown Heights, NY 10598	1
Robert Schwartz NWC Code 38504 Naval Weapons Center China Lake, CA	1	Prof. Gar B. Hoflund Chemical Engineering 227 Chemical Engineering Building Gainesville, FL 32611	1
T. S. Sudarshan Materials Modification, Inc. P. O. Box 4817 Falls Church, VA 22044	1	Dr. A. T. Collins Wheatstone Physics Laboratory King's College London, Strand London WC2R 2LS UNITED KINGDOM	1
Wally Yarbrough Penn State University 271 MRL University Park, PA 16802	1		